Peroxisomal import stress activates integrated stress response and inhibits ribosome biogenesis

Jinoh Kim [ID][a,3], Kerui Huang [ID][a,1,3], Pham Thuy Tien Vo [ID][a,2], Ting Miao[a,1], Jacinta Correia [ID][a], Ankur Kumar [ID][a], Mirre J. P. Simons [ID][b] and Hua Bai [ID][a,*]

[a]Department of Genetics, Development, and Cell Biology, Iowa State University, Ames, IA 50011, USA
[b]Department of Animal and Plant Sciences and Bateson Centre, The University of Sheffield, Sheffield S10 2TN, United Kingdom
[1]Present address: Department of Genetics, Blavatnik Institute, Harvard Medical School, Boston, MA 02115, USA
[2]Present address: Division of Biological Sciences, University of California San Diego, San Diego, CA 92093, USA
*To whom correspondence should be addressed: Email: hbai@iastate.edu
[3]J.K. and K.H. contributed equally to this work.
Edited By Christian Metallo

Abstract

Impaired organelle-specific protein import triggers a variety of cellular stress responses, including adaptive pathways to balance protein homeostasis. Most of the previous studies focus on the cellular stress response triggered by misfolded proteins or defective protein import in the endoplasmic reticulum or mitochondria. However, little is known about the cellular stress response to impaired protein import in the peroxisome, an understudied organelle that has recently emerged as a key signaling hub for cellular and metabolic homeostasis. To uncover evolutionarily conserved cellular responses upon defective peroxisomal import, we carried out a comparative transcriptomic analysis on fruit flies with tissue-specific peroxin knockdown and human HEK293 cells expressing dominant-negative PEX5^{C11A}. Our RNA-seq results reveal that defective peroxisomal import upregulates integrated stress response (ISR) and downregulates ribosome biogenesis in both flies and human cells. Functional analyses confirm that impaired peroxisomal import induces eIF2α phosphorylation and ATF4 expression. Loss of ATF4 exaggerates cellular damage upon peroxisomal import defects, suggesting that ATF4 activation serves as a cellular cytoprotective mechanism upon peroxisomal import stress. Intriguingly, we show that peroxisomal import stress decreases the expression of rRNA processing genes and inhibits early pre-rRNA processing, which leads to the accumulation of 47S precursor rRNA and reduction of downstream rRNA intermediates. Taken together, we identify ISR activation and ribosome biogenesis inhibition as conserved adaptive stress responses to defective peroxisomal import and uncover a novel link between peroxisomal dysfunction and rRNA processing.

Keywords: PEX5, peroxisomal import stress, integrated stress response, ribosome biogenesis, early rRNA processing

Significance Statement

The ability to sense and respond to defective organelle protein import is crucial in maintaining cellular homeostasis. Here, through comparative transcriptomic analysis on fruit flies and human cell cultures, we show that defective peroxisomal import upregulates integrated stress response (ISR) and downregulates ribosome biogenesis. Intriguingly, the activation of ATF4 by peroxisomal import stress is not dependent on classical eIF2α kinases, suggesting a distinct eIF2α-independent mechanism for ATF4 activation. Furthermore, peroxisomal import stress specifically downregulates early pre-rRNA processing, a unique cellular response that has not been reported in any previous organelle stresses. Together, the activation of ISR and the inhibition of ribosome biogenesis may serve as an adaptive mechanism to maintain protein homeostasis and cellular fitness upon peroxisomal import stress.

Introduction

Eukaryotic cells contain various membrane-bound subcellular compartments, such as the endoplasmic reticulum (ER), mitochondria, and peroxisomes. Proteins that reside in each organelle are mainly synthesized on cytosolic ribosomes and imported to the organelles by elaborate machinery (1). Impaired protein import into organelles elicits a number of cellular stress responses,

including adaptive pathways to maintain protein homeostasis. Generally, cellular stress responses downregulate anabolic processes and employ energetic reserves for pro-survival functions. In line with this notion, unfolded protein response (UPR) in ER or mitochondria inhibits protein translation to reduce the workload and activates transcriptional induction of chaperones or proteases to maintain protein homeostasis (2, 3). Also, mistargeting

of mitochondrial proteins activates UPR^{am} (UPR activated by protein mistargeting) to reduce global translation and increase the proteasomal activity to modulate the proportion of unimported precursor proteins in the cytosol (4, 5). In addition, inhibition of mitochondrial import induces the expression of Cis1, which is associated with the mitochondrial translocase, to prevent the accumulation of mitochondrial precursor protein at the mitochondrial translocase as a surveillance mechanism (6). Moreover, it has been shown that blockage of mitochondrial import by a "clogger" protein immediately activates a global transcriptional program to restore cellular proteostasis (7). However, mechanisms underlying the response to impaired protein targeting in other organelles, including peroxisomes, are poorly understood.

Peroxisomes are central metabolic organelles in almost all eukaryotic cells (8, 9). The organelles play an essential role in lipid metabolism, including beta-oxidation of very long-chain fatty acids and alpha-oxidation of branched fatty acids, biosynthesis of ether phospholipid and bile acid (8). Moreover, peroxisomes play a crucial role in detoxifying reactive oxygen species (ROS) due to their abundance of antioxidant enzymes, such as catalase (Cat) (10). Given that peroxisomes are important in human physiology, genetic defects of peroxisomal biogenesis or the absence of functional peroxisomes are associated with severe pathology in humans (11–13). For example, patients with Zellweger syndrome, the most severe peroxisomal biogenesis disorder, exhibit craniofacial dysmorphism, hepatic dysfunction, and neurological abnormalities (11, 12). In addition, emerging studies suggest that impaired peroxisomal functions increase the risk of obesity and its complications (14, 15). Lastly, dysregulated peroxisomal import function has recently been linked to aging (16, 17), cancer (18), viral infection, immune response (19, 20), and neurodegeneration (21, 22).

Peroxisomal matrix enzymes are post-translationally imported into the organelles from the cytosol. Unlike other organelles with enclosed membranes, peroxisomes can import folded enzymes, and then they seem to lack intraperoxisomal chaperones (23, 24). Most of the cargo proteins contain peroxisome targeting signals type 1 (PTS1) sequence at the C-terminus consisting of a serine–lysine–leucine (SKL) motif or a conservative variant (25, 26). PTS1 proteins are transported to the peroxisomes by the shuttling receptor PEX5. The cargo-receptor complex binds to the peroxisomal membrane proteins PEX13 and PEX14. After docking, the cargo proteins are translocated across the peroxisomal membrane and imported into the lumen, while receptor protein PEX5 is then mono-ubiquitinated at the cysteine 11 site by E3 ubiquitin ligases PEX2, PEX10, and PEX12. The PEX1–PEX6 complex releases ubiquitinated PEX5 from the peroxisomal membrane to the cytosol, and PEX5 is deubiquitinated by USP9X in mammalian systems for the next cycle of transport (26–28).

Several recent studies have found that peroxisomal protein import is compromised with age (16, 17, 29–33). For instance, cat is observed to be mislocalized to the cytosol in aged cells and replicative senescent cells (31, 33). Our previous studies show that peroxisomal import activities are significantly decreased in aged fly hepatocytes (16, 30). However, the precise contribution of impaired peroxisomal import to the loss of cellular homeostasis during aging remains largely unknown. Interestingly, a recent study has unveiled peroxisomal retrograde signaling in *Caenorhabditis elegans* (34). The authors discovered that peroxisomal import stress triggers transcriptional upregulation of peroxisomal Lon protease *lonp-2/LONP2* and catalase *ctl-2/CAT* through NHR-49/PPARα and its co-factor MDT-15/MED15 (34). Nonetheless, whether this retrograde signaling observed in worms is conserved in mammals remains unclear.

This study aims to identify evolutionarily conserved cellular responses to peroxisomal import deficiency through a comparative transcriptomic analysis between fruit flies and human cells. Our RNA-seq results reveal that peroxisomal import stress triggers the induction of integrated stress response (ISR) and inhibition of ribosome biogenesis in both flies and humans. Functional analyses show that defective peroxisomal import induced markers of ISR, such as eIF2α phosphorylation and ATF4 translation, consistent with previous studies using *Pex2* knockout mice (35, 36). Additionally, we observe that peroxisomal import stress downregulates the expression of ribosomal RNA (rRNA) processing genes and inhibits the early processing of 47S precursor rRNA. Thus, our study uncovers previously undefined cellular stress responses to defective peroxisomal import and links peroxisomal import stress to ribosome biogenesis and protein homeostasis.

Results
Generation of peroxisomal import stress in human cells and flies

Despite the emerging importance of peroxisomes in regulating aging and diseases, little is known about how cells cope with peroxisomal dysfunction. The cellular stress responses to defective peroxisomal import are largely uncharacterized. To study peroxisome import stress responses, we generated an inducible peroxisomal import blockage system in the mammalian cell culture. In this system, we knocked in Tet-ON 3G tetracycline-inducible expression construct into the AAVS1 safe harbor locus in human embryonic kidney-derived HEK293 cells. The inducible expression construct contained a FLAG-tagged full-length human PEX5 with a single amino acid substitution at position 11 (cysteine to alanine, C11A), a conserved ubiquitination site for PEX5 recycling and peroxisomal protein import (Fig. 1A and B). PEX5 is the receptor that recognizes cargo proteins containing peroxisomal targeting signal type 1 (PTS1) and delivers them to the peroxisomal matrix through docking complex PEX13/PEX14. After releasing its cargo, PEX5 is mono-ubiquitinated through the E3 ubiquitin ligase complex PEX2/PEX10/PEX12 and then released from the peroxisome membrane by the AAA-ATPases PEX1 and PEX6. In the cytosol, the ubiquitin moiety is removed, and PEX5 becomes available for another round of import (13, 37) (Fig. 1A).

It has shown that stable expression of PEX5^{C11A} mutant exerts a dominant-negative effect on wild-type PEX5 recycling and efficiently blocks peroxisomal import in mammalian cell culture (38). In our inducible system, the PEX5^{C11A} mutant protein level was robustly induced by treating cells with increasing concentrations of doxycycline (Dox), 0.1–1 μg/mL, but not in wild-type HEK293 cells (Fig. 1C). Induction of the PEX5^{C11A} mutant was able to block peroxisomal import (marked by GFP-PTS1 reporter) without affecting peroxisomal number (marked by PEX14) (Fig. 1D, E and G). Furthermore, we noticed that the peroxisomal import was effectively blocked (70%) 24 h post Dox treatment and completely blocked (100%) by 48 h post Dox treatment, even though the highest induction of PEX5^{C11A} mutant protein and cell growth defect were observed in 72 h (Fig. S1). Interestingly, unimported PTS1 signals were accumulated in the cytosol, which may cause the imbalance of protein homeostasis (Fig. 1F).

To identify evolutionarily conserved pathways involved in peroxisomal stress responses, we also silenced peroxins in *Drosophila* oenocytes, the hepatocyte-like cells containing high
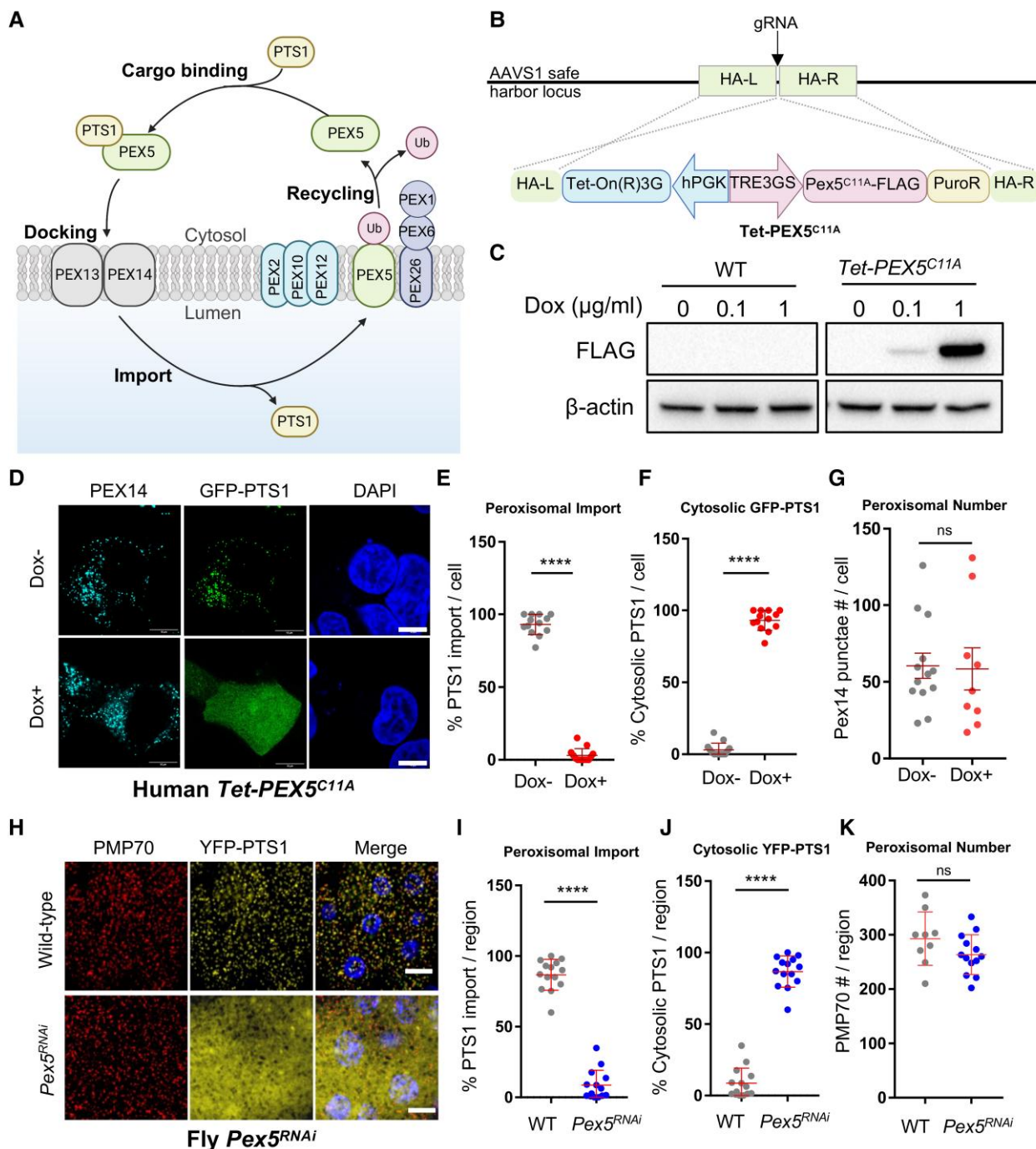
Fig. 1. Targeting PEX5 to generate peroxisomal import stress in human HEK293 cells and *Drosophila* oenocytes. A) Simplified model of peroxisomal import machinery in humans. PTS1: peroxisomal targeting signal of type 1. B) Schematic diagram for the generation of tetracycline-inducible $PEX5^{C11A}$ knock-in HEK293 cell line (Tet-PEX5^{C11A}). FLAG is tagged at the C-terminal of the $PEX5^{C11A}$ sequence. C) Western blot to verify the $PEX5^{C11A}$ expression in WT and Tet-PEX5^{C11A} cells. 0.1 or 1 μg/mL of Dox was treated for 3 days. D) Immunostaining showing peroxisomal import activity in human Tet-PEX5^{C11A} cells with or without 1 μg/mL of Dox treatment for 3 days. Scale bar: 10 μm. E–G) Quantification of the percentage GFP-PTS1 import per cell (E), percentage unimported cytosolic GFP-PTS1 per cell (F), and peroxisomal number (marked by PEX14) per cell (G) of (D). H) Immunostaining showing peroxisomal import activity in *Drosophila* oenocytes of wild-type (−RU) and $Pex5^{RNAi}$ (+RU). *PromE-GS-Gal4* driver used for inducible oenocyte-specific *Pex5* knockdown. (I-K) Quantification of the percentage of imported YFP-PTS1 per region (I), percentage of unimported YFP-PTS1 (J), and the number of peroxisome marked by PMP70 per region (K) of (H). All experiments are presented as mean ± SD; t test; ****$P < 0.0001$; ns, not significant; $N = 10$–15.

amounts of peroxisomes (30, 39). Previously, we reported that knocking down *Pex5* in oenocytes shows increased ROS and the production of inflammatory cytokines (30). We utilized an oenocyte-specific GeneSwitch driver (*PromE^{GS}-Gal4*) to transiently knock down peroxin genes in the adult oenocytes. RU486 (mifepristone, or RU) activated *PromE^{GS}-Gal4* (+RU). Knockdown

of *Pex5* in *Drosophila* oenocyte significantly blocked peroxisomal import (indicated by YFP-PTS1 reporter) without altering peroxisomal number (marked by Pmp70/Abcd3) (Fig. 1H, I, and K). Like the mammalian system, unimported YFP-PTS1 reporter proteins accumulated in the cytosol upon *Pex5* knockdown (Fig. 1J).

Transcriptomic analysis reveals conserved peroxisomal stress responses in human cells and *Drosophila* oenocytes

Then, we performed transcriptomic analysis from human Tet-PEX5[C11A] cells and Drosophila Pex5 knockdown oenocytes to characterize cellular responses induced by defective peroxisomal import. RNA-seq analysis was carried out using human Tet-PEX5[C11A] cells treated with or without Dox for 3 days and oenocytes dissected from flies fed with or without RU486 for 5 days (Fig. 2A).

Our RNA-seq analysis revealed great transcriptional responses in PEX5[C11A] expressing HEK293 cells with 4,426 upregulated differentially expressed genes (DEGs) and 3,009 downregulated DEGs (fold-change >1.2, FDR < 0.1) (Fig. 2B, File S1). On the other hand, *Pex5* knockdown in fly oenocytes produced 1,059 DEGs (587 upregulated and 472 downregulated) (fold-change >1.2, FDR < 0.1) (Fig. 2C and Fig. S2). To our surprise, most of the peroxisome biogenesis genes and peroxisomal matrix enzymes were not significantly upregulated in response to defective peroxisomal import in human PEX5[C11A] cells, except for peroxisomal Lon peptidase 2 (LONP2) (Fig. S2). In fly oenocytes with *Pex5* knockdown, although no peroxisome biogenesis genes were significantly upregulated upon peroxisomal import stress, we found four matrix enzymes were induced by *Pex5* knockdown, hydroxyacid oxidase, acyl-CoA oxidase (Acox57D-p, ACOX1), Cat, and xanthine dehydrogenase (ry) (Fig. S2). These results suggest that peroxisomal retrograde signaling might be activated upon peroxisomal import stress, consistent with a recent study (34). The downstream targets of the peroxisomal retrograde signaling appear to differ across species or among different cell types.

To uncover the conserved cellular processes that were differentially regulated by PEX5 mutants, we conducted gene ontology (GO) analysis on identified DEGs. Human PEX5[C11A] specifically induced transcriptional regulation, apoptotic process, actin cytoskeleton organization, Wnt signaling, MAPK cascade, ER unfolded protein response (UPR[ER]), and Hippo signaling (Fig. 2D, File S3). In contrast, PEX5[C11A] downregulated translation (including mitochondrial translation), mRNA splicing, rRNA processing, ribosome biogenesis, mitochondrial respiration, and fatty acid beta-oxidation (Fig. 2E, File S3).

Fly *Pex5* knockdown upregulated transmembrane transport, proteolysis, actin cytoskeleton organization, defence response, response to ER stress, and immune system process (Fig. 2F, file S3), while downregulated rRNA processing, ribosome biogenesis, lipid metabolism, hydrogen peroxide catabolic process, and oxidant detoxification (Fig. 2G, File S3). Through the GO analysis, we identified several common pathways altered upon defective peroxisomal import in both humans and flies. For example, both PEX5 mutants upregulate cytoskeleton organization, immunity and inflammatory response, and ER stress response, while downregulated mitochondrial respiration, lipid metabolism, and ribosome biogenesis including rRNA processing and ribosomal assembly.

Besides the shared pathways, we found 811 conserved DEGs between humans and flies (Fig. 3A). For example, genes in ER stress were upregulated, such as *HSP90AB1/Hsp83* (human vs. fly), *SEC61A1/Sec61alpha*, *SYVN1/sip3*, *DNAJB12/CG3061*, *HSPA1A/ Hsc70-3*. In contrast, genes involved in ribosome biogenesis are downregulated, including *UTP6/CG7246*, *NOP10/CG7637*, *FBL/Fib*, *NOP58/nop5*, *NOP58/Nop56*, *REXO5/Rexo5*, and *CG9107/RRP7A*. In addition, Gene Set Enrichment Analysis (GSEA) on both PEX5 mutants in fly and humans further confirmed that defective peroxisomal import specifically upregulated ER UPR and ISR pathways, while downregulated ribosome biogenesis and rRNA processing (Fig. 3B and C). Together, these results suggest that peroxisomal import stress perturbs protein homeostasis, which leads to the induction of ER and ISR and inhibition of ribosome biogenesis in both flies and humans.

To determine whether the transcriptional changes observed above are general peroxisomal import stress response or are specific to the loss of *Pex5*, we conducted additional RNA-seq analysis on fly oenocytes with knockdown of *Pex1* or *Pex12*. Previous studies demonstrated that reducing the expression of both *Pex1* and *Pex12* led to impaired peroxisome import, although *Pex1* knockdown caused a stronger peroxisomal import defect than *Pex12* knockdown (30, 40). Consistent with these studies, we found that the knockdown of *Pex1* induced 1,008 DEGs, whereas the knockdown of *Pex12* only induced 235 DEGs (fold-change >1.2, FDR < 0.1) (Fig. S3A, File S4). A pairwise comparison of the transcriptional changes among three *Pex* knockdowns indicated that *Pex5* knockdown exhibited gene expression profiles more similar to *Pex1* knockdown ($r = 0.18$), compared with *Pex12* ($r = 0.092$) (Fig. S3B). Even though the transcriptional changes were not identical among 3 *Pex* knockdowns (Fig. S3A), ER pathway was differentially regulated in all 3 knockdowns (Fig. S3C), as well as ribosome biogenesis and assembly (Fig. S3D and E, File S5). Thus, the differential regulation of ER stress and ribosome biogenesis does not only respond to the loss of *Pex5*; rather it is a general stress response to peroxisomal import defects.

Although the link between peroxisomal impairment and ER stress responses has been previously reported (35, 36), we decided to conduct a detailed analysis to deepen our understanding of the ER stress and ISR pathways as a conserved cellular responses to peroxisomal dysfunction. Additionally, since the connection between peroxisomes and ribosome biogenesis has not been studied before, we further investigated the mechanism by which peroxisomal import stress downregulates ribosomal biogenesis.

Peroxisomal import stress activates the ISR

Our transcriptomic analysis revealed that ER stress response pathways are upregulated among all 3 Pex knockdowns (*Pex1*, *Pex5*, and *Pex12*) in *Drosophila* and PEX5[C11A] in humans. The ER stress pathways are mediated through 3 stress sensors, including inositol-requiring protein 1 (IRE1), protein kinase RNA-like ER kinase (PERK), and activating transcription factor 6 (ATF6) (2) (Fig. 4A). IRE1 splices the transcription factor XBP1 pre-mRNA into its mature form, which is translocated to the nucleus to induce the transcription of molecular chaperone genes (41). PERK phosphorylates the α subunit of eukaryotic initiation factor 2 (eIF2) at serine 51, which blocks the exchange of eIF2-GDP to eIF2-GTP and global translation (42, 43). Phosphorylated eIF2α (p-eIF2α) selectively enhances the translation of ATF4, a transcription activator of genes essential for adaptive responses (44, 45). The ATF6 branch is responsible for the transcriptional induction of the ER chaperone genes (46).

To test whether ER stress is indeed induced by defective peroxisomal import, we first examined the IRE1-XBP1 branch. We employed an *Xbp1-EGFP* reporter in *Drosophila* to measure Ire-1 mediated splicing activity (47). Consistent with previous studies, *Xbp1* splicing was enhanced to produce in-frame EGFP expression upon treating dithiothreitol (DTT), a potent ER stress inducer (Fig. 4B and C). Surprisingly, the *Xbp1-EGFP* reporter was not induced by *Pex5* knockdown fly oenocytes (Fig. 4B and C). Similarly, the spliced-XBP1 (sXBP1) levels remained unchanged in human cells expressing PEX5[C11A] mutant proteins (Fig. 4D
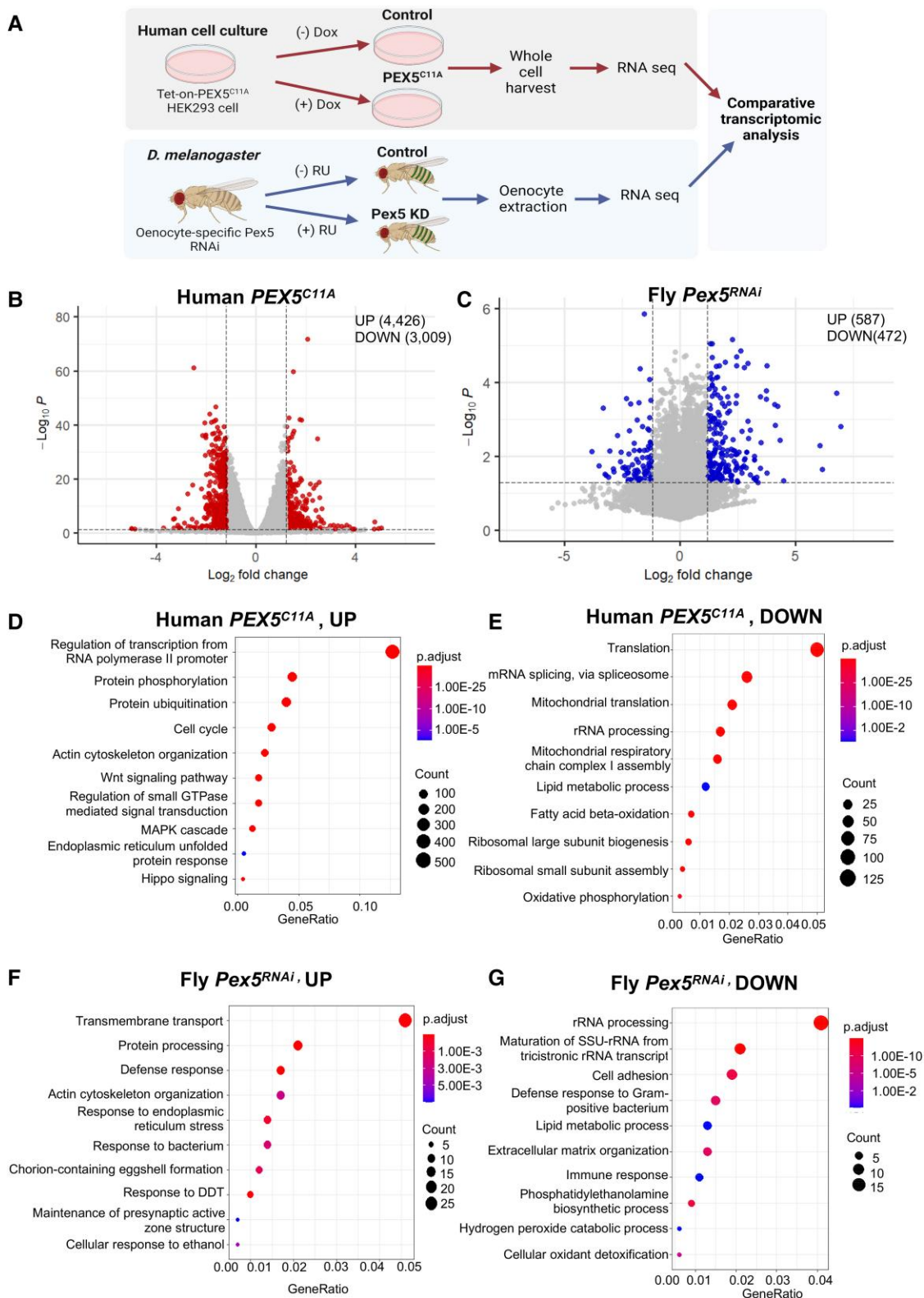
Fig. 2. Transcriptomic analysis on peroxisomal stress response in human Tet-PEX5[C11A] cells and *Pex5* knockdown flies. A) Schematic diagram showing RNA-seq analysis in both human cell culture and fly oenocytes. B) Volcano plot for human PEX5[C11A] RNA-seq (FDR < 0.1, FC > 1.2). C) Volcano plot for *Drosophila* Pex5[RNAi] RNA-seq (FDR < 0.1, FC > 1.2). D) Dot plot showing upregulated biological processes in human cells expressing *PEX5[C11A]* (Dox+) compared with control condition (Dox−). E) Dot plot showing downregulated biological processes in human cells expressing *PEX5[C11A]* (Dox+) compared with control condition (Dox−). F) Dot plot showing upregulated biological processes in fly *Pex5* knockdown oenocytes compared with wild-type. G) Dot plot showing downregulated biological processes in fly *Pex5* knockdown oenocytes compared with wild-type.

Fig. 3. Activation of ER stress response and inhibition of ribosome biogenesis are conserved peroxisomal stress responses. 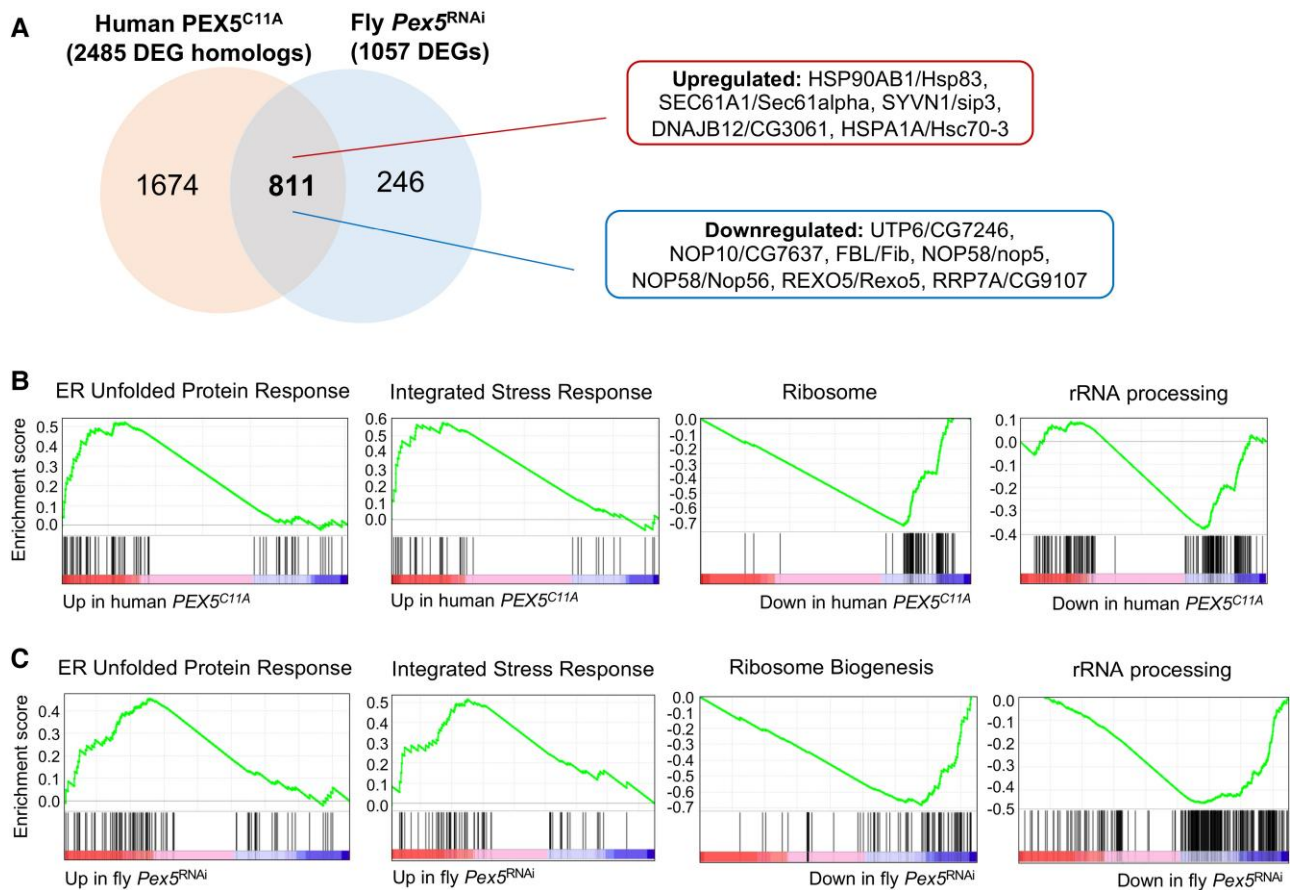A) Venn diagram showing the overlapping DEGs (FDR < 0.1, FC > 1.2) between human PEX5^{C11A} and fly Pex5^{RNAi}. Genes belong to ER stress are shown in the red box. Shared ribosome biogenesis genes are shown in the blue box. B) GSEA showing the enrichment of ER unfolded stress response and ISR among all upregulated pathways in human PEX5^{C11A} cells, while ribosome and rRNA processing are enriched among all downregulated pathways. C) Similarly, GSEA showing the same enrichment of ER unfolded stress response, ISR, ribosome biogenesis, and rRNA processing in Pex5^{RNAi} flies.

and E). Our finding is consistent with a previous study where *Pex2* knockout mice showed no changes in IRE1α signaling and its RNase activity, but the PERK pathway and ATF4 transcriptional activities were activated in the liver of *Pex2* knockout mice (35). Similarly, we found the cleavage of ATF6 was only slightly activated, but not significantly, upon peroxisomal import stress in human cells (Fig. 4F–H). Due to the lack of fly Atf6 antibody, we did not test the ATF6 branch in the fly model.

We then examined the PERK branch by measuring the phosphorylation of eIF2α in both *Pex5* knockout flies and PEX5^{C11A} expressing human cells. Contrary to IRE1-XBP1 and ATF6 pathways, we observed a significant increase in phosphorylation of eIF2α upon peroxisomal import deficiency in both flies (Fig. 4I and J) and human cells (Fig. 4K and L). In line with these observations, we also found that the protein expression of ATF4 was highly induced in human PEX5^{C11A} mutants (Fig. 4K and M). The potential compounding effect of Dox (1 μg/mL) was excluded, since Dox treatment alone did not induce eIF2α phosphorylation and ATF4 expression in wild-type HEK293 cells (Fig. 4K–M). These results suggest that peroxisomal import stress activates a specific branch of ER stress pathways, the PERK-eIF2α-ATF4 axis.

The eIF2α and ATF4 are also known as the core regulators of ISR and they mediate cellular adaptation to a variety of stress conditions, including ER stress (48, 49). Four known mammalian protein kinases phosphorylate eIF2α: PKR-like ER kinase (PERK),

heme-regulated eIF2α kinase (HRI), double-stranded RNA-dependent protein kinase (PKR), and general control nonderepressible 2 (Fig. 4A). Each kinase is activated by distinct stress stimuli (50). We then wondered which eIF2α kinase is responsible for the induction of eIF2α phosphorylation upon peroxisomal import stress. To address this question, we knocked down the four known eIF2α kinases individually in Tet-PEX5^{C11A} cells using siRNAs (Fig. S4) and after that treated the cells with Dox to trigger peroxisomal import stress. We found that only PERK knockdown attenuated the phosphorylation of eIF2α induced by PEX5^{C11A} expression (Fig. 5A and B). Intriguingly, none of the eIF2α kinase knockdowns blocked the induction of ATF4 upon peroxisomal import stress (Fig. 5A and C). ATF4 can be induced through eIF2α-independent pathways, such as mitochondrial stress response (51, 52) and mTORC1 signaling (53–55). Although no kinase knockdown affects the ATF4 induction, ISR inhibitor (ISRIB) treatment (56, 57) blocked ATF4 induction under peroxisomal stress (Fig. 5D and E), indicating independent mechanisms for eIF2α phosphorylation and ATF4 activation.

It is known that ATF4 responds to oxidative stress as a redox-regulated transcription factor (58–60). Previously, we showed that impaired peroxisomal function induces ROS production in *Pex5* mutant flies (30). We verified that PEX5^{C11A} expressing human cells also showed elevated intracellular ROS levels (Fig. S5A and B). We then wonder whether ROS can activate ATF4
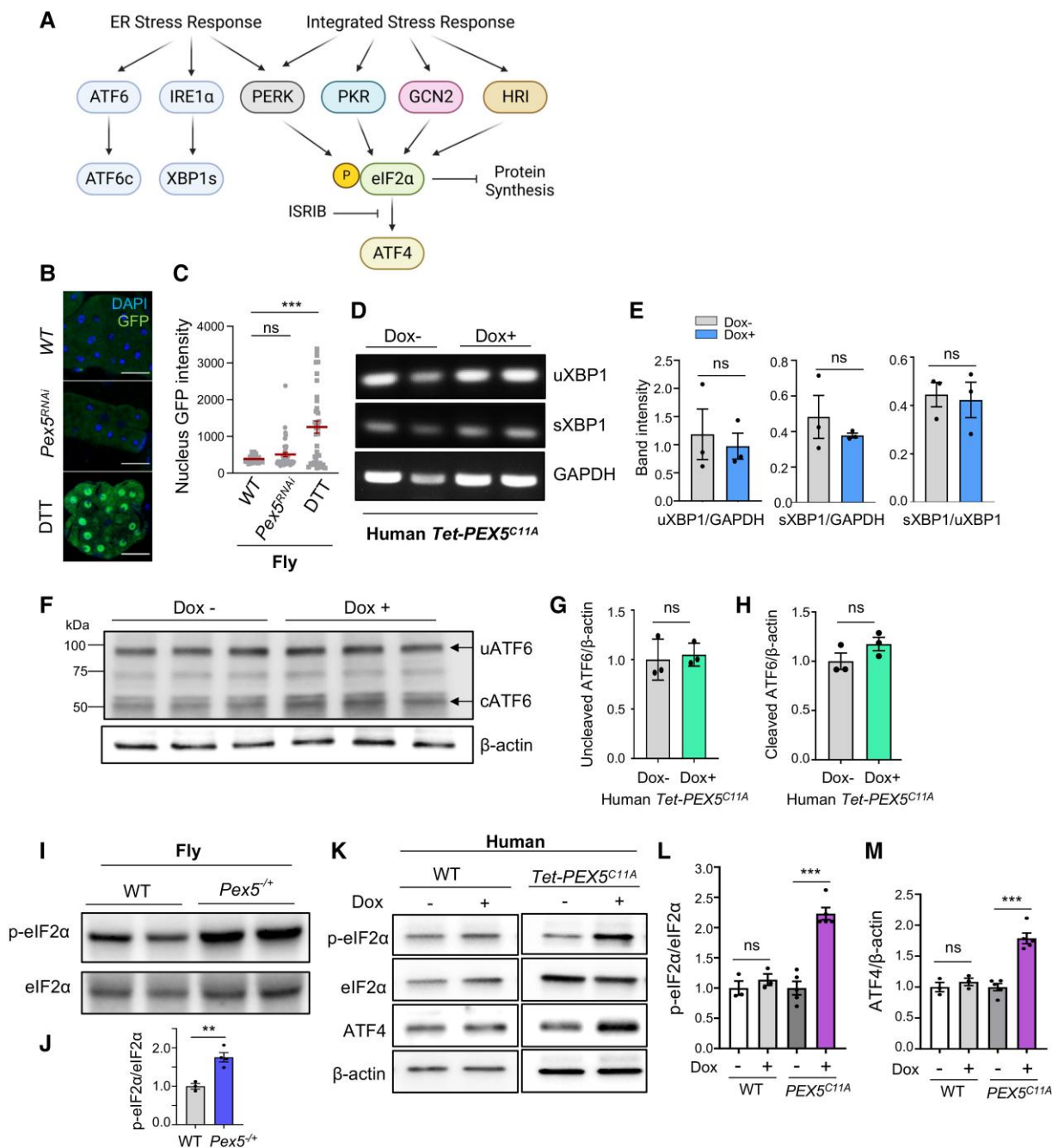
Fig. 4. Peroxisomal import stress activates p-eIF2α-ATF4 axis, but not XBP1 and ATF6 branches of the ER stress response pathway. A) Schematic diagram of ER stress response and the ISR pathways. B) Immunostaining of fly oenocytes expressing *Xbp1-EGFP* splicing reporter upon *Pex5* knockdown and DTT treatment. Scale bar: 20 μm. C) Quantification of nucleus GFP intensity of (B). Data are presented as mean ± SD; one-way ANOVA; Tukey's multiple comparison test: ***P < 0.001; ns, not-significant; N = 3. D, E) RT-PCR analysis of unspliced-XBP1 (uXBP1) and sXBP1 in human PEX5^{C11A} cells treated with or without Dox (1 μg/mL). Data are presented as mean ± SD; t test; ns, not significant; N = 3. F–H) Western blotting showing ATF6 cleavage human PEX5^{C11A} cells treated with or without Dox (1 μg/mL). Data are presented as mean ± SD; t test; ns, not significant; N = 3. I, J) Western blotting showing phosphorylation of eIf2α (p-eIF2α) in wild-type and *Pex5$^{-/+}$* mutant flies. Data are presented as mean ± SD; t test; **, P < 0.01; N = 3. K–M) Western blotting showing p-eIF2α and ATF4 expression in human PEX5^{C11A} cells treated with or without Dox (1 μg/mL). Data are presented as mean ± SD; one-way ANOVA; Tukey's multiple comparison test: ***P < 0.001; ns, not significant; N = 3–5.

expression upon peroxisomal import stress. To test this, we treated *PEX5^{C11A}* expressing human cells with a ROS scavenger, *N*-acetyl-L-cysteine (NAC). We observed that peroxisomal import stress increased mRNA and protein expression of Nuclear Factor Erythroid 2-Related Factor 2 (NRF2), a key antioxidant regulator under oxidative stress (61), while the NAC treatment blocked *PEX5^{C11A}*-mediated induction of NRF2 (Fig. S5C–E). Intriguingly,

NAC treatment did not block the induction of ATF4 upon peroxisomal import stress, although it reduced the basal levels of ATF4 (Fig. 5F–H). Together, these results suggest that peroxisomal import stress activates ATF4 through an unknown mechanism independent of eIF2α kinases and ROS signaling.

Previously, we have reported impaired peroxisomal import function in aged fly oenocytes (30). This led us to investigate whether ISR
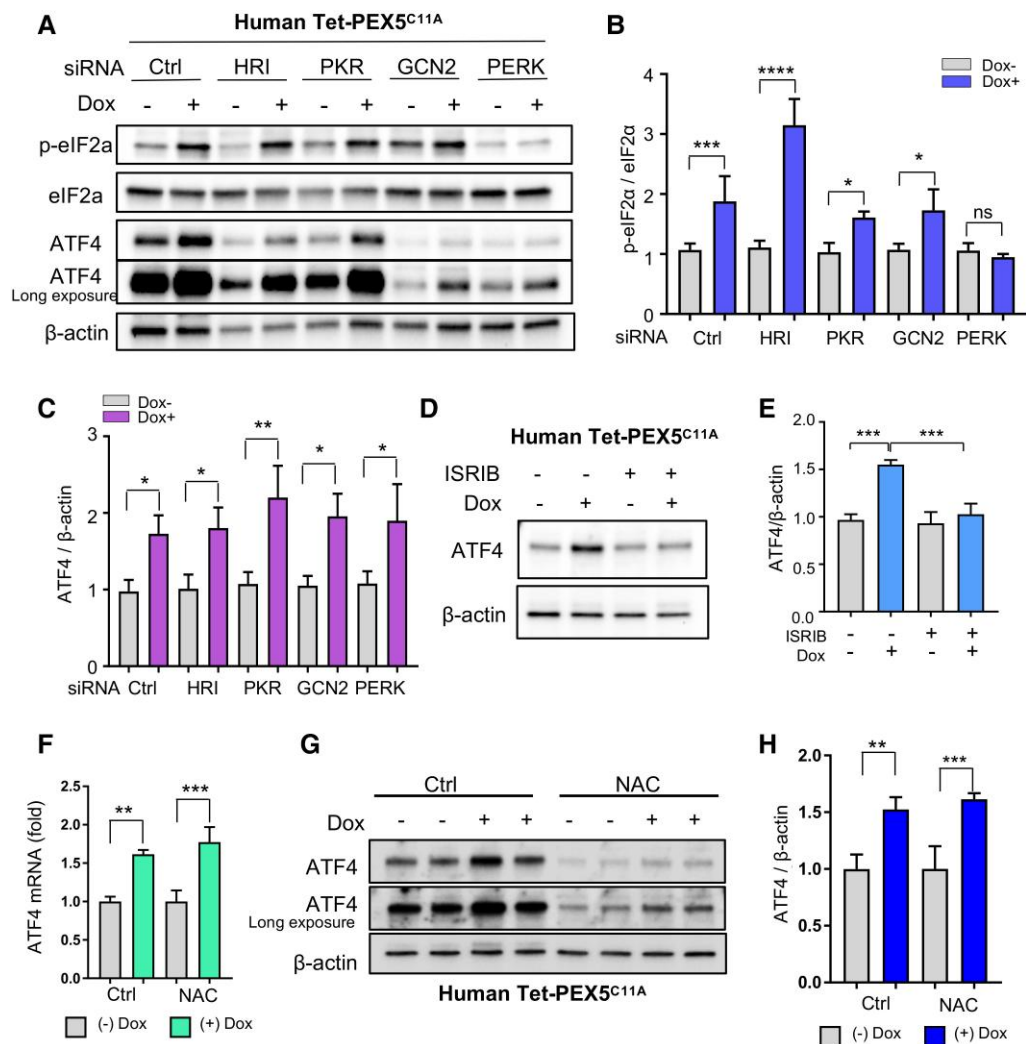
Fig. 5. ATF4 is activated through the ISR pathway in response to defective peroxisomal import. A–C) Western blotting showing phosphorylation of eif2α (p-eIF2α) and ATF4 expression in human Tet-PEX5^{C11A} cells with the knockdown of the 4 eIF2α kinases. Data are presented as mean ± SD; one-way ANOVA; Tukey's multiple comparison test: *$P < 0.05$; ***$P < 0.001$; ****$P < 0.0001$; ns, not significant; $N = 3$. Statistical differences were calculated by comparing with dox-group of each knockdown condition. D, E) Western blotting showing ATF4 expression in human Tet-PEX5^{C11A} cells treated with ISR inhibitor (ISRIB, 500 nM). ISRIB was added one day before Dox treatment. Data are presented as mean ± SD; one-way ANOVA; Tukey's multiple comparison test: ***$P < 0.001$; $N = 3$. F) ATF4 mRNA expression by qRT-PCR of human Tet-PEX5^{C11A} cells treated with 4 mM NAC. NAC was administered 3 h prior to Dox treatment, which lasted for 48 h. Data are presented as mean ± SD; one-way ANOVA; Tukey's multiple comparison test: **$P < 0.01$; ***$P < 0.001$, $N = 3$. G, H) Western blot analysis showing ATF4 expression in human Tet-PEX5^{C11A} cells treated with 4 mM NAC. NAC was pretreated 3 h prior to Dox treatment, which lasted for 48 h. Data are presented as mean ± SD; one-way ANOVA; Tukey's multiple comparisons test: **$P < 0.01$; ***$P < 0.001$; $N = 3$.

and ATF4 are upregulated in aged flies. Analysis of oenocyte-specific translatome in young (1-week-old) and aged (4-week-old) flies (16) showed significant upregulation of ISR genes in aged oenocytes (Fig. S6A). Additionally, we found that the protein expression of ATF4 was induced in aged flies (Fig. S6B and C). These findings demonstrate that the ISR-ATF4 pathway, associated with peroxisomal dysfunction, is linked to the aging process.

Induction of ATF4 by peroxisome import stress is cytoprotective

ATF4 serves as a central regulator of metabolic and oxidative homeostasis as well as cell survival (62), through the transcriptional regulation of genes in amino acid transport, metabolism, protein homeostasis, and antioxidant (62). However, ATF4 has also been implicated in promoting apoptosis, cell-cycle arrest, and senescence under persistent cellular stress (3, 62, 63). In our

transcriptomic analysis, we observed upregulation of many ATF4 target genes, including molecular chaperones like *HSPA1A* and *HSPA1B* in humans and *Hsp70Ba, Hsp70Bb, Hsp70Bc* in flies, in response to peroxisomal import stress (Fig. 6A). Consistent with the increased ATF4 translation shown in Fig. 5, ATF4 mRNA expression was significantly elevated in *PEX5*^{C11A} mutant cells (Fig. 6B). We hypothesized that the induction of ATF4 might serve as an adaptive mechanism to protect cells from peroxisomal import stress. We showed that 3 days of *PEX5*^{C11A} expression led to a 20% reduction in cell number, while *ATF4* knockdown further reduced the cell number under peroxisomal import stress (Fig. 6C). To assess whether the decreased cell number is due to enhanced cell death, we quantified live and dead cells using LIVE/DEAD cell imaging kit (Fig. 6D and E). We found that the cells with peroxisomal import stress only exhibited mild cell death. However, the extent of cell death was further exacerbated by *ATF4* knockdown under peroxisomal import stress, underscoring the essential role
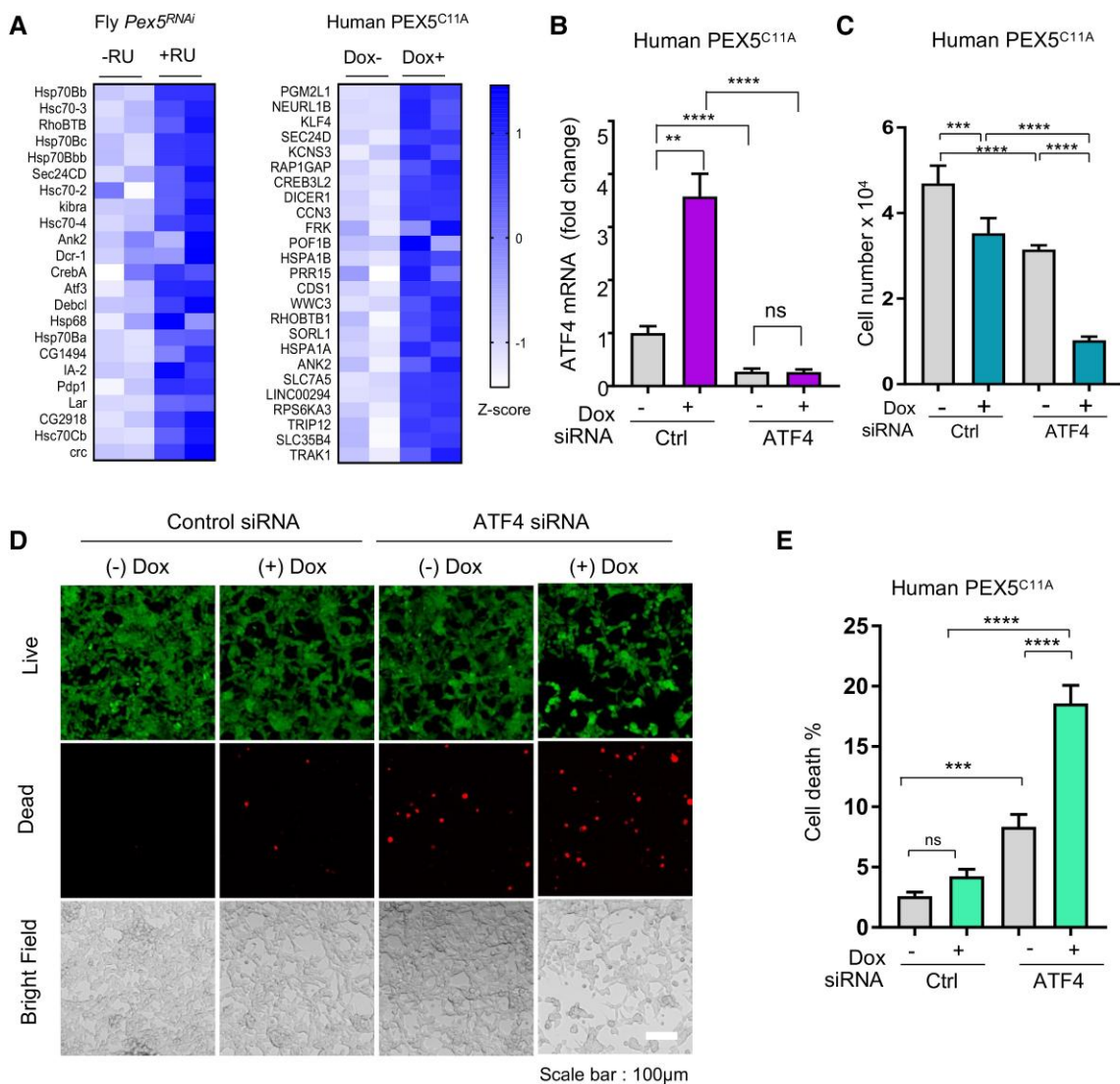
Fig. 6. Induction of ATF4 by peroxisome import stress is cytoprotective. A) Heatmap showing upregulation of ATF4 target genes in both fly *Pex5* knockdown and human PEX5[C11A] cells. ATF4 target gene set is retrieved from GSEA. B) *ATF4* mRNA expression by qRT-PCR of human Tet-PEX5[C11A] cells with the knockdown of *ATF4*. Data are presented as mean ± SD; one-way ANOVA; Tukey's multiple comparison test: **$P < 0.01$; ****$P < 0.001$, ns, not significant, $N = 3$. C) Cell number was counted after 3 days of dox (1 μg/mL) treatment with ATF4 knockdown in human Tet-PEX5[C11A] cells. Data are presented as mean ± SD; one-way ANOVA; Tukey's multiple comparison test: ***$P < 0.001$; ****$P < 0.0001$; $N = 6$. D) ATF4 knockdown cells were stained with a LIVE/DEAD cell Imaging kit. Live cells were detected by the green channel, whereas dead cells were detected by the red channel. E) Quantification of the percentage of dead cells in the total cell of (D). Data are presented as mean ± SD; one-way ANOVA; Tukey's multiple comparison test: ***$P < 0.001$; ****$P < 0.0001$; $N = 5$.

of ATF4 in maintaining cell fitness, particularly in response to peroxisomal dysfunction. Since intracellular ROS is elevated upon peroxisomal import stress (Fig. S5A and B), we wonder whether ROS scavengers can rescue *ATF4* knockdown-induced cell death. We surprisingly found that NAC treatment showed no effects on cell death induction associated with *ATF4* knockdown (Fig. S5F), which again suggests a ROS-independent regulation of ATF4 during peroxisome import stress. Together, these findings suggest that ATF4 activation represents a cytoprotective mechanism to sustain cell fitness under peroxisomal import stress.

Peroxisomal import stress inhibits ribosome biogenesis, especially early rRNA processing

Ribosomes are macromolecular complexes assembled with rRNA and ribosomal proteins that function as mRNA translation machines (64). In humans, the 80S ribosome consists of a small 40S subunit and a large 60S subunit. The small 40S subunit contains 18S rRNA and 33 ribosomal proteins, while the large 60S subunit contains 28S, 5.8S, and 5S rRNAs as well as 47 ribosomal proteins (r-proteins) (64, 65) (Fig. 7). Ribosome biogenesis is the most energy-demanding process in cellular activities. It involves all three nuclear RNA polymerases and sequential rRNA modification and processing steps (65) (Fig. S7A). The process takes place mainly in the nucleolus and is initiated by transcription of preribosomal RNA (pre-rRNA) through RNA polymerase I (Pol I), from which the mature 18, 5.8, and 28S rRNAs are generated (Fig. 7).

Our comparative transcriptomic analysis revealed that the ribosome biogenesis pathway was downregulated upon peroxisomal import stress in both human cells and fly hepatocytes, particularly the genes involved in rRNA modifications and processing (Fig. 7 and Fig. S7B, C). For example, peroxisomal import stress
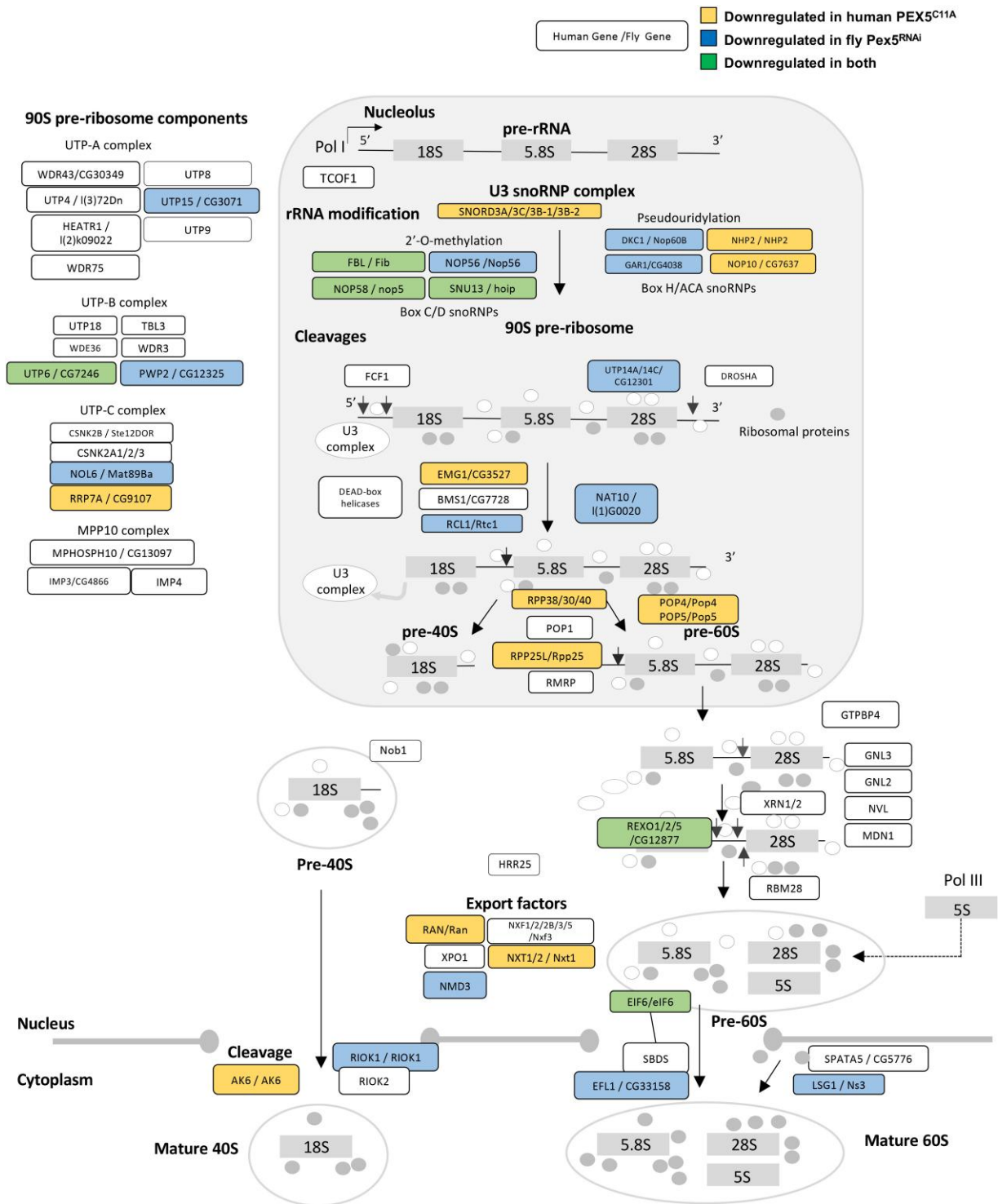
Fig. 7. Ribosome biogenesis is downregulated upon peroxisomal import stress. Schematic diagram showing ribosome biogenesis pathway (adapted from the KEGG pathway). Human genes and their fly homologs are separated by slash. Genes that are downregulated only in human PEX5[C11A] cells are highlighted in yellow. Genes that are downregulated only in fly *Pex5*[RNAi] are highlighted in blue. Genes that are downregulated in both human PEX5[C11A] cells and fly *Pex5*[RNAi] are highlighted in green.

downregulated genes involved in rRNA modification (*FBL/Fib, NOP58/Nop5, NOP56/Nop56, SNU13/hoip, NOP10/CG7637,* and *DKC1/Nop60B*) and rRNA processing (*EMG1/CG3527, RCL1/Rtc1, NAT10/l(1)G0020, POP4/Pop4, POP5/Pop5,* and *REXO5/CG33158*) (Fig. 7). We performed qRT-PCR analysis to validate the expression of a few candidate genes identified from the RNA-seq. Interestingly, most of the downregulated ribosome biogenesis

genes are linked to early rRNA modification and processing in both flies and human cells (e.g. *FBL/Fib, NOP58/Nop5,* and *NOP10/CG7637*) (Fig. 8A and B), suggesting that early steps of rRNA processing are specifically targeted by peroxisomal import stress.

Next, we sought to verify our findings on peroxisomal stress-regulated rRNA processing using northern blot and specific RNA
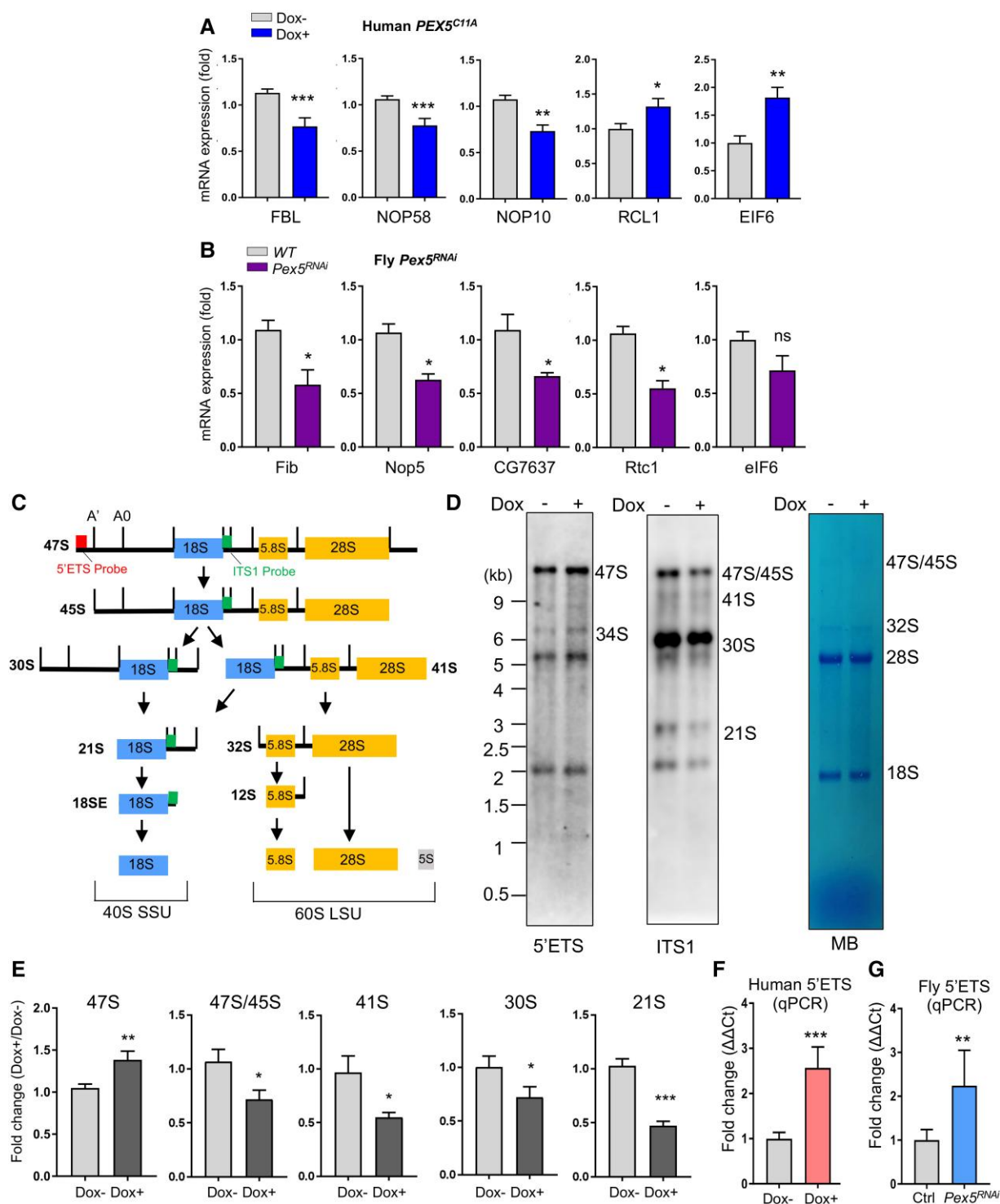
Fig. 8. rRNA processing is inhibited in response to defective peroxisomal import. A) Quantitative RT-PCR showing the expression of rRNA processing genes upon Dox treatment in human PEX5^{C11A} cells. Data are presented as mean ± SD; t test: *$P < 0.05$; **$P < 0.01$; ***$P < 0.001$; $N = 3$. B) Quantitative RT-PCR showing the expression of rRNA processing genes in fly oenocytes with Pex5 knockdown. Data are presented as mean ± SD; t test: *$P < 0.05$; ns, not significant; $N = 3$. C) Schematic diagram of the rRNA processing and maturation pathway. Approximate locations of northern blotting probes are noted in red (5'ETS) and green (ITS1). D) Northern blot showing different rRNA intermediates in human PEX5^{C11A} cells with or without Dox treatments. Methylene blue staining was shown for equal RNA loading. E) Band intensity of rRNA intermediates was normalized to 18S rRNA and the fold-change between Dox+ and Dox− treatments was presented. Data are presented as mean ± SD; t test: *$P < 0.05$; **$P < 0.01$; ***$P < 0.001$; $N = 3$–4. F) Quantitative RT-PCR analysis on the expression of human 47S pre-rRNA after Dox treatment. Data are presented as mean ± SD; t test; ***$P < 0.001$; $N = 4$. G) Quantitative RT-PCR analysis on the expression of 47S pre-rRNA in Pex5 knockdown flies. Data are presented as mean ± SD; t test; **$P < 0.01$; $N = 4$.

probes to visualize various rRNA intermediates. The human primary pre-rRNA, 47S rRNA, is synthesized by RNA Pol I. 47S rRNA is polycistronic, containing 18, 5.8, and 28S rRNAs, flanked by

the 5′ and 3′ external transcribed spaces (5′ and 3′ ETS) and two internal transcribed spacers (ITS1 and ITS2). This pre-rRNA must be processed by multiple enzymes to release mature

rRNAs (Fig. 8C). We first carried out a northern blot analysis to characterize the changes in various rRNA intermediates upon peroxisomal import stress. Our northern blot analysis using an ITS1 probe revealed a significant decrease in most of the processing intermediates (45, 41, 30, 26, and 21S rRNAs) upon peroxisomal import stress (Fig. 8D and E). Intriguingly, the northern blots using the 5′ETS probe showed slightly, but significantly, increased levels of the full 47S pre-rRNA in PEX5^{C11A} expressing cells (Fig. 8D and E). The 5′ETS is located at the extreme 5′ end of the 47S pre-rRNA and is not present in the downstream 45S rRNA intermediates (Fig. 8C). Thus, the 5′ETS can be used to precisely monitor the level of the full 47S pre-rRNA. The reduced downstream rRNA intermediates and increased 47S pre-rRNA observed from our northern blot analysis suggest that peroxisomal import stress might inhibit an early pre-rRNA processing step converting 47S pre-rRNA to 45S rRNA, potential through repressing the cleavage of 5′ETS sequence at the A′ site. Furthermore, we confirmed the 47S rRNA accumulated phenotypes using qRT-PCR and primers targeting 5′ETS in both human PEX5^{C11A} cells and fly oenocytes with *Pex5* knockdown (Fig. 8F and G). Additionally, we observed 47S rRNA accumulation and downregulation of rRNA processing genes in old flies, suggesting that the downregulation of early rRNA processing is linked to the aging process (Fig. S7D). Together, these results demonstrate that early rRNA processing is inhibited upon peroxisomal import stress, leading to an accumulation of 47S pre-rRNA and a decrease in downstream intermediates.

Protein synthesis is inhibited in response to defective peroxisomal import

The mammalian target of rapamycin complex 1 (mTORC1) signaling is well-established for its pivotal role in protein translation and ribosome biogenesis (66, 67). Among its best-understood substrates downstream of mTORC1 are the ribosomal protein S6 (RPS6) kinases (S6K1/2) and the protein initiation factor 4E binding proteins. As a serine/threonine kinase, mTORC1 phosphorylates S6K1, thereby enhancing ribosomal DNA transcription. Moreover, mTORC1/S6K1 regulates mRNA translation at both initiation and elongation stages. Additionally, 4E-BP1, another critical translation initiation factor downstream of mTORC1, plays a role in mRNA translation. Phosphorylation of 4E-BP1 leads to its release from eIF4E, allowing cap-dependent translation to proceed (66).

Given that ribosome biogenesis is altered upon peroxisomal dysfunction, we wondered whether mTORC1 signaling is also targeted by peroxisomal import stress. Our western blot analysis revealed that the phosphorylation of both S6K1 and 4E-BP1 was significantly downregulated in human PEX5^{C11A} cells (Fig. 9A–C), suggesting a potential inhibition of global protein synthesis and reduction of rRNA transcription. These findings further suggest that the accumulation of 47S pre-rRNA observed in response to peroxisomal import stress is mainly attributed to the inhibition of early rRNA processing, despite the downregulation of rRNA synthesis.

Finally, we investigated whether peroxisomal stress-regulated inhibition of ribosome biogenesis affects global protein synthesis using a puromycin incorporation assay. Puromycin, a structural analog of aminoacyl tRNAs, is incorporated into nascent polypeptide chains during translation, thereby preventing elongation (68, 69). A minimal amount of puromycin is incorporated into neosynthesized proteins, directly reflecting the mRNA translation rate in vitro (68, 70). We treated Dox for 3 days on PEX5^{C11A} cells, followed by brief incubation (10 min) with puromycin before protein extraction. Global translation was measured by western blotting

with an antibody against puromycin. As expected, we found that peroxisomal import stress significantly inhibited global protein synthesis (Fig. 9D and E). The reduction of global protein synthesis under peroxisomal import stress might be attributed to a combination of ISR activation and ribosome biogenesis inhibition (Fig. 9F).

Discussion

Peroxisome is the central metabolic site for detoxification of hydrogen peroxide, β-oxidation of very long-chain fatty acids, and ether phospholipid biosynthesis. Emerging studies have suggested that peroxisomes are the novel regulator of animal aging and society-impacting diseases such as cancer, viral infection, diabetes, and neurodegeneration (15, 71). Peroxisomal function, in particular peroxisomal import, is known to be impaired during aging. However, how cells mount adaptive responses to cope with defective peroxisomal import remains to be established. Here, we conduct a comparative transcriptomic analysis to profile transcriptional changes under peroxisomal import stress in both fruit flies and human cell cultures. We identified that defective peroxisomal import activates the ISR pathway and induces eIF2α phosphorylation and ATF4, a critical regulator for cellular fitness and protein homeostasis. In addition, peroxisomal import stress downregulates ribosome biogenesis, especially in early rRNA processing. Our work uncovers a conserved adaptive mechanism that protects cells from peroxisomal import stress and maintains cellular protein homeostasis (Fig. 9F).

Although we did not find many peroxisome genes that are upregulated in response to defective peroxisomal import, we uncovered two conserved cellular responses in both flies and human cell culture, the activation of ISR and downregulation of ribosome biogenesis. Both stress responses are likely used by the cells to cope with loss of protein homeostasis and accumulation of unimported peroxisomal proteins. Here, we show that peroxisomal import stress specifically activates the phosphorylation of eIF2α signaling, but not the XBP1 or ATF6 branches of the ER stress pathway. These results are consistent with a previous study wherein *Pex2* knockout mice exhibited unchanged IRE1α signaling and its RNase activity, but the PERK pathway and ATF4 transcriptional activities were activated in the liver of *Pex2* knockout mice (35). Additionally, we found that the upstream regulation of eIF2α phosphorylation and ATF4 is not identical despite defective peroxisomal import inducing both eIF2α phosphorylation and ATF4 expression. Although the translation of ATF4 is known to be regulated through p-eIF2α (48, 49), emerging evidence suggests that ATF4 expression can be regulated independently from the PERK-p-eIF2α axis. It has been shown that ATF4 was required for only 7.5% of ER UPR genes, whereas PERK was required for nearly 50% of UPR responses from previously published RNA-seq studies (72, 73), indicating distinct regulations and functions of ATF4 from PERK-p-eIF2α signaling.

ATF4 is one of the master regulators of cellular stress response (62). However, persistent stress conditions promote ATF4 to induce apoptosis (3, 63, 74). To examine the role of ATF4 activation in peroxisomal import stress response, we measured cellular fitness and cell death upon peroxisomal stress and ATF4 depletion. Our results suggest that ATF4 is critical for maintaining cellular fitness upon peroxisomal stress because cells with *ATF4* knockdown are more sensitive to peroxisomal import stress. These findings are consistent with the role of ATF4 in transcriptional activation of the genes involved in resistance to oxidative stress (59, 60). Thus, activation of ATF4 represents an adaptive
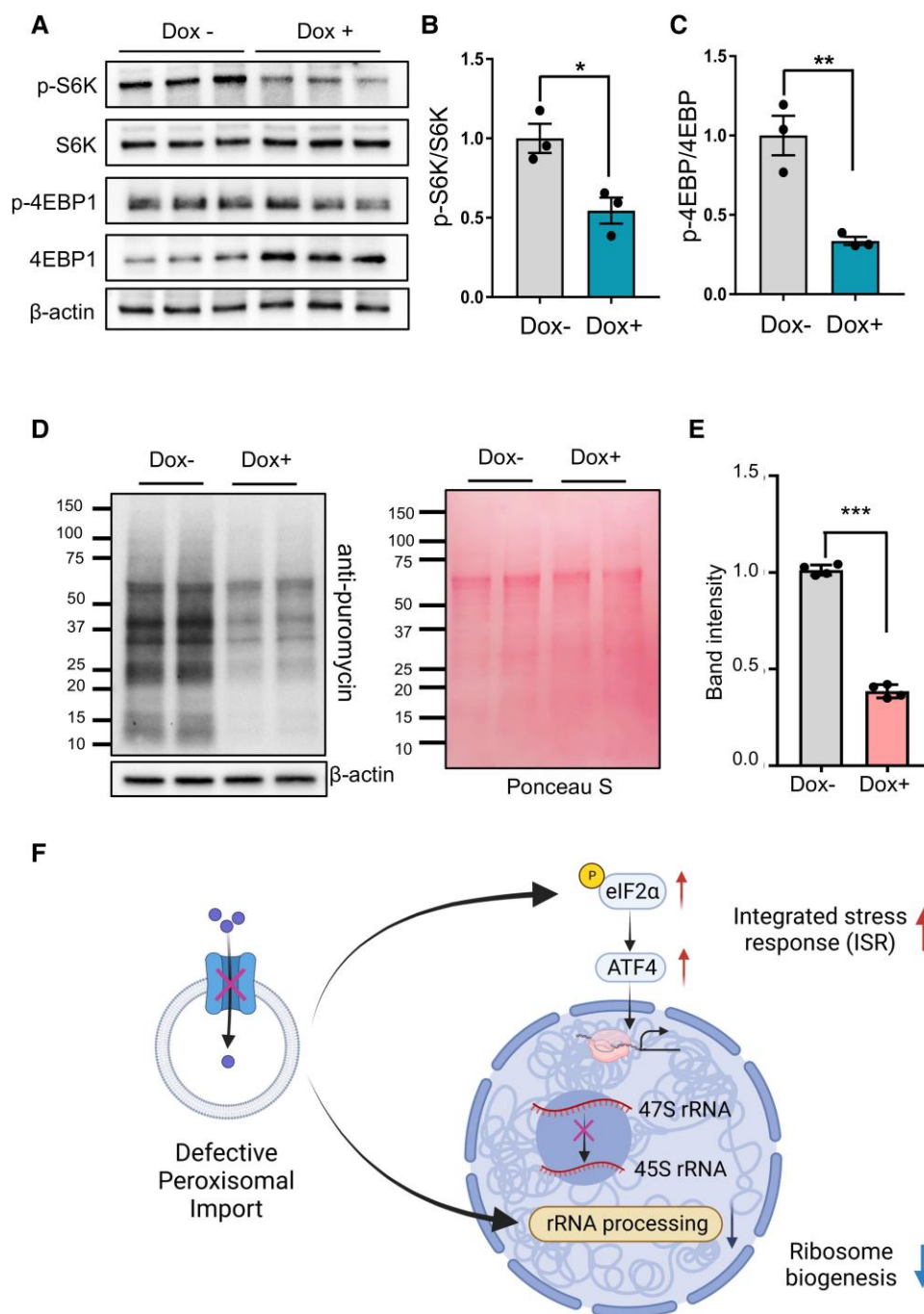
Fig. 9. Protein synthesis is diminished upon peroxisomal import stress. A) Western blotting analysis of mTOR signaling by monitoring the phosphorylation of S6K (p-p70S6K) and 4EBP1 (p-4EBP1) in human PEX5^{C11A} cells. B) Quantification of phosphorylation of S6K band intensity normalized by S6K. Data are presented as mean ± SD; t test: *$P < 0.05$; $N = 3$. C) Quantification of phosphorylation of 4EBP1 band intensity normalized by 4EBP1. Data are presented as mean ± SD; t test: **$P < 0.01$; $N = 3$. D) Puromycin incorporation assay in human Tet-PEX5^{C11A} upon Dox treatment. Human Tet-PEX5^{C11A} cells were incubated with or without Dox for 3 days, following by addition of 10 μg of puromycin for 10 min. Western blotting was carried out using an antibody against puromycin. β-Actin blot and Ponceau S staining were shown for equal protein loading. E) Quantification of western blot antibody against puromycin. Band intensity is normalized by β-actin. Data are presented as mean SD; t test; ***, $P < 0.001$; $N = 4$. F) Model showing ribosomal biogenesis inhibition and ISR activation as two conserved cellular responses to defective peroxisomal import (Created with BioRender.com).

mechanism that protects cells from the damage induced by peroxisomal import stress. Intriguingly, despite the elevated intracellular ROS under peroxisomal import stress, ROS scavenger NAC did not can block peroxisomal dysfunction-mediated ATF4 activation. This finding highlights a ROS-independent mechanism for ATF4 activation upon peroxisomal import stress.

Eukaryotic ribosome biogenesis is a highly complex event that involves 80 ribosomal proteins, more than 200 nonribosomal proteins, and 75 small nucleolar RNAs (75). The defect of ribosome biogenesis at various steps can promote cell-cycle arrest, senescence, or apoptosis (76). In this regard, impaired ribosome biogenesis is linked with cancer, aging, and aging-related degenerative diseases, even though the exact mechanisms need further study (76–78). Through our transcriptomic analysis, we find significantly decreased gene expression involved in ribosome biogenesis in both fly and human PEX5 mutants, particularly those involved

in rRNA processing. Our northern blotting analysis further shows that peroxisomal import stress specifically inhibits A′ cleavage in the 5′ETS of 47S pre-rRNA. Ribosome RNA processing is highly regulated and involves the modification and cleavage of the precursor rRNA and the packaging and assembly of the rRNA into ribosome subunits (79). However, the exact mechanism for A′ cleavage of 47S pre-rRNA remains elusive. Interestingly, a recent study (80) reported that A′ cleavage of 47S pre-rRNA is inhibited upon the treatment of sodium arsenite (NaAsO2), an ISR inducer (81, 82). The authors hypothesize that the unprocessed pre-rRNA is stored within the nucleolus until the stress has resolved, at which point it can reenter the ribosome biogenesis pathway. Likewise, the peroxisomal import stress might trigger a similar retention of the pre-rRNA pool during the early adaptive response phase. This pre-rRNA can be quickly released for ribosome biogenesis once the peroxisomal import stress is resolved. Further studies are needed to investigate this possibility. Given that sodium arsenite represses A′ cleavage of 47S pre-rRNA, the ISR signaling (e.g. ATF4) could be one of the promising candidates in mediating pre-rRNA processing upon peroxisomal import stress. Furthermore, it has been well-established that reduced ribosome proteins and ribosome biogenesis factors can increase longevity in model organisms (see (76) for review). Thus, ribosome biogenesis inhibition can be a protective mechanism to confer peroxisomal stresses.

mTOR is a crucial regulator of cellular growth and promotes protein synthesis by activating S6 kinases or keeping 4E-BP proteins in an inactivated state to halt translation elongation. S6 kinase phosphorylates several downstream targets, including the RPS6, a component of the 40S ribosomal subunit. Phosphorylation of RPS6 by S6 kinase is thought to facilitate ribosome biogenesis by increasing the synthesis of rRNA and other components of the ribosome. Thus, mTOR activity is highly linked with ribosome biogenesis. Interestingly, the mTOR pathway is downregulated upon peroxisomal import stress in human $PEX5^{C11A}$ cells, suggesting a potential decrease in rRNA synthesis. This finding further supports the idea that early pre-rRNA processing is specifically inhibited by peroxisomal import stress. We speculate that the peroxisomal import stress might trigger the retention of 47S pre-rRNA, which could be quickly released and processed for ribosome biogenesis once the stress is resolved. Although numerous efforts have gone to identify the rRNA processing factors, the enzyme responsible for cleavage at the A′ site of the 5′ETS is still not fully established. Identifying this undefined enzyme and understanding how it regulates the pre-rRNA process will provide an essential insight into this unique cellular stress response in the nucleolus.

Peroxisomes communicate with other organelles, including mitochondria and ER, through membrane contact sites or peroxisome-derived metabolites (28). In agreement with peroxisome-center inter-organelle communication, our transcriptomic analysis identifies many organelle-specific gene expression changes, especially the genes involved in ER and mitochondrial function. Peroxisomes are highly linked with the mitochondria in diverse metabolic and cellular processes such as β-oxidation of fatty acids, redox homeostasis, and inflammatory responses (83). In this regard, it has been reported that the loss of functional peroxisomes causes mitochondrial dysfunction (83–87). For example, patients with peroxisomal biogenesis disorders exhibit altered inner mitochondrial membrane structure and reduced respiratory chain complex activities (87). Similarly, liver-specific *Pex5*-knockout mice showed the functional decline of respiratory chain complexes I, III, and V, reduced membrane potential, increased ROS production, and morphological changes in mitochondria (84). Our transcriptomic analysis revealed that the oxidative phosphorylation pathway is downregulated upon

$PEX5^{C11A}$ expression. For example, the expression of genes in complexes I–IV of the respiratory chain is downregulated upon peroxisomal import stress. These results suggest that mitochondrial electron transport activity is significantly impaired under peroxisomal stress, consistent with previous publications (86, 88, 89). Activation of the ATF4 pathway also occurs under mitochondrial import stress (52, 90). Mitochondrial stress, induced by OXPHOS inhibitors leads to HRI-dependent ATF4 activation in human cells (90). In contrast to these previous studies, we observed under peroxisomal import stress ATF4 induction is independent of eIF2α kinases and ROS signaling, suggesting a noncanonical regulation is involved. Our finding is aligned with previous research showing that ATF4 can be activated by FCCP even when eIF2α kinases are depleted (52), or by mTORC1 signaling under mitochondrial stress (53–55).

It is known that ISR-ATF4 activation is a common cellular response to many cellular stresses, including mitochondrial and ER stress. It is not a surprise that peroxisomal import defects can also active ISR-ATF4 pathway. However, the downregulation of ribosome biogenesis upon impaired peroxisomal import, in particular early rRNA processing, has not been observed under other organelle dysfunctions yet. Although recent transcriptome analysis reveals that mitochondrial protein import defects downregulates the expression of 80S ribosome components (7), it remains to be determined whether mitochondrial stress specifically inhibits early rRNA processing as what we observed in peroxisomal import stress. Given the functional connection between peroxisomes and mitochondria, it is possible that the induction of ISR-ATF4 and the downregulation of ribosome biogenesis are the common cellular responses to both peroxisomal and mitochondrial dysfunction.

In summary, we uncover two evolutionarily conserved pathways as the cellular stress responses to defective peroxisomal import. We show that peroxisomal import stress activates the ISR pathway to induce ATF4, a cytoprotective mechanism to protect cells from damage associated with peroxisomal defects. Moreover, we provide the first evidence that peroxisomal import stress downregulates rRNA processing and inhibits A′ cleavage of 47S pre-rRNA. Finally, we observed activation of ISR-ATF4 pathway and downregulation of ribosome biogenesis in aged flies. We expect that our study will contribute to a better understanding of peroxisomal stress response and possible therapeutic strategies for peroxisome-associated diseases, such as metabolic disorders, neurodegenerative disease, and aging.

Materials and methods

Detailed reagent information is provided in the Table of Reagents.

Plasmid construction

Human *PEX5* cDNA was purchased from Dharmacon Mammalian Gene Collection. The *hPEX5* was amplified by PCR using the forward and reverse primers (5′-CACTATAGGGAGACCCAAGCT TATCTAGACATGGCAATGCGGGAGCT-3′ and 5′-TCTTACTTGTCA TCGTCGTCCTTGTAGTCGCCCTGGGGCAGGCC-3′) and introduced between XhoI and BamHI sites in c-Flag pcDNA3 (Addgene #20011) to generate Flag-tagged hPEX5 using NEBuilder HiFi DNA assembly Master mix (New England Biolabs). Site-directed mutagenesis for amino acid substitution (cysteine to alanine at position 11, C11A) was performed using the Q5 Site-directed mutagenesis kit (New England Biolabs) according to the manufacturer's instruction. The primers for the $PEX5^{C11A}$ mutant were 5′-GGAGGCCGAAgctGGGGGTGCCA ACC-3′ and 5′-ACCAGCTCCCGCATTGCC-3′. To generate

tetracycline-inducible $PEX5^{C11A}$ plasmid, we modified pMK243 (Tet-OsTIR1-PURO) from Masato Kanemaki (Addgene #72835). pMK243 was digested by BgIII and MluI to remove the OsTIR sequence. Flag-PEX5^{C11A} was amplified by PCR using the forward and reverse primers (5′-gattatgatcctctagacatatgctgcagattactt gtcatcgtcgtccttgtagt-3′ and 5′-tcctaccctcgtaaagaattcgcggccgcaa tggcaatgcgggagctggt-3′) and introduced between BgIII and MluI sites in digested pMK243 plasmid to generate Tet-PEX5^{C11A}-PURO plasmid. All plasmids are confirmed by Sanger sequencing. GFP-tagged PTS1 plasmid was purchased from Addgene (#54601).

Generation of CRISPR knock-in HEK293 cells expressing PEX5^{C11A}

HEK293 cells were cultured in Dulbecco's Modified Eagle Medium containing 10% fetal bovine serum, with penicillin and streptomycin. Cells were incubated in a 37 °C incubator in an atmosphere of 5% CO2 in air. To generate a stable cell line, we followed the protocol described by Natume et al. (91). 1×10^6 HEK293 cells were plated in one well of a 6-well plate. After 24 h, 800 ng of AAVS1 T2 CRISPR in pX330 (Addgene #72833) and 1 μg of Tet-PEX5^{C11A}-PURO were transfected using Effectene (Qiagen) according to the manufacturer's instructions. After 48 h, the cells were detached and diluted at 10 to 100 times in 10 mL of selection medium containing 1 μg/mL of puromycin. The cells were seeded in a 10 cm dish and the selection medium was exchanged every 3 to 4 days. After 8 to 10 days, colonies were marked using a marker pen under a microscope, picked by pipetting with 10 μL of trypsin-EDTA, and subsequently transferred to a 96-well plate containing 100 μL of the selection medium. The cells were allowed to grow until confluency and subcultured 24-well plates and 6-well plates. The cells containing correct $PEX5^{C11A}$ knock-in were identified through PCR genotyping.

Genomic DNA isolation and PCR

To extract genomic DNA, cells were first lysed in buffer A solution (100 mM Tris-HCl [pH 7.5], 100 mM EDTA, 100 mM NaCl, 0.5% SDS) followed by incubation at 65 °C for 30 min. Buffer B (1.43 M potassium acetate, 4.28 M lithium chloride) was then added and incubated on ice for 10 min. After centrifuging at 12,000 rpm for 15 min, the supernatant was transferred to a new microtube with isopropanol. Precipitated genomic DNA was washed in 70% ethanol and resuspended with DNase-free water. To verify Tet-PEX5^{C11A}-PURO insertion into the AAVS1 locus, genomic PCR was performed using Q5 High-Fidelity DNA polymerase (New England BioLabs). Primers for WT cell validation are: 5′-cgtttcttaggatggccttc-3′ and 5′-agaagg atggagaaagagaa-3′. Primers for Tet-PEX5C11A-PURO integration are: 5′-cgtttcttaggatggccttc-3′ and 5′-ccgggtaaatctccagagga-3′.

Fly husbandry and strains

Female flies were used in all experiments. Flies were maintained at 25 °C, 60% relative humidity, and a 12-h light/dark cycle. Adults and larvae were reared on a standard cornmeal and yeast-based diet (0.8% cornmeal, 10% sugar, and 2.5% yeast). Fly stocks used in this study were as follows: $Pex5^{[MI06050]}/FM7h$ (BDSC #44685), UAS-$Pex5^{RNAi}$ (BDSC #58064), UAS-$Pex1^{RNAi}$ (BDSC #28979), and UAS-$Pex12^{RNAi}$ (BDSC #53308). The control line used for the KD experiments is yw^R (a gift from Marc Tatar). Gene-switch driver $PromE800$-GS-$Gal4$ (a gift from Heinrich Jasper) was used to drive oenocyte-specific gene knockdown. Gene KD was achieved by feeding flies on 100 μM of RU486 food (Mifepristone, Cayman Chemical #100063171) for 5–6 days.

Fly oenocyte RNA isolation

Adult female oenocytes (20 tissues per replicate) were dissected in cold 1× PBS before RNA extraction. For oenocyte dissection, we first removed fat body through liposuction and then detached oenocytes from the cuticle using a small glass needle. Tissue lysis, RNA extraction was performed using RNeasy Micro kit (QIAGEN, #74034) with the following modifications. Tissues were pooled in 1.7 mL centrifuge tube containing 150 μL of Buffer RLT and 143 mM β-mercaptoethanol on ice during the dissection. Samples were then incubated at room temperature (RT) for 3 min. 150 μL buffer RLT was added and tissues were homogenized using pellet pestle grinder (Kimble pellet pestles, #749540-0000).

RNA-seq and bioinformatics

RNA-seq libraries were constructed using 100 ng of total RNA and NEBNext Ultra II RNA Lib Prep kit (NEB, Ipswich, MA, USA. #E7770L). RNA concentrations were measured using Qubit RNA BR Assay Kit (Thermo Fisher Scientific, #10210). Poly(A) mRNA was isolated using NEBNext Oligo d(T)25 beads and fragmented into 200 nt in size. Purification of the ligation products are performed using Beckman Coulter AMPURE XP (BECKMAN COULTER, #A63880). After cDNA synthesis, each cDNA library was ligated with a NEBNext adaptor and barcoded with an adaptor-specific index (NEBNext Multiplex Oligos for Illumina, NEB, #E7335S). Twelve libraries were pooled in equal concentration and sequenced using Illumina HiSeq 3000 platform (single end, 150 bp reads format).

FastQC (v0.11.8) was first performed to check the sequencing read quality. Sequence alignment and mapping were performed using the Spliced Transcripts Alignment to a Reference (STAR) software (v2.7.3a) (92). The raw reads were mapped to *D. melanogaster* genome (BDGP Release 6) or Genome Reference Consortium Human Build 38 (GRCh38). Reads mapped were then counted with summarized Overlaps function using "Union" mode in R. Counts are then analyzed in DESeq2 (v1.26.0) (93) for batch control analysis and test for differential expression. RNA-seq read files have been deposited to NCBI's Gene Expression Omnibus (GEO) (Accession #GSE167197).

GO and pathway analysis were performed with DAVID (91). For GSEA analysis, text was trimmed and organized using Java script. Normalized counts were used as input for parametric analysis and organized as suggested by GSEA tutorial site (94). Collapse dataset to gene symbols was set to false. Permutation type was set to gene set; number of permutations was set to 1,000; enrichment statistic used as weighted analysis; metric for ranking genes was set to signal to noise.

Quantitative real-time polymerase chain reaction

Quantitative real-time polymerase chain reaction (qRT-PCR) was performed using Quantstudio 3 Real-Time PCR system and SYBR green master mixture (Thermo Fisher Scientific, USA #A25778). All gene expression levels were normalized to RpL32 (in *Drosophila*), GAPDH (in humans) by the method of comparative Ct (95). Mean and standard errors for each gene were obtained from the averages of three biological replicates, with two technical repeats. RT-PCR primers are listed below.

Immunostaining and peroxisomal import assay

For fly peroxisomal import assay, a YFP-PTS1 reporter expressed transiently in fly oenocytes using $PromE$-GS-$Gal4$ (with 1-day RU486 feeding). Adult oenocyte tissues were dissected in 1× PBS

and fixed in 4% paraformaldehyde for 15 min at RT. Tissues were washed with 1× PBS with 0.3% Triton X-100 (PBST) for three times (~5 min each time) and blocked in PBST with 5% normal goat serum for 30 min. Tissues were then incubated overnight at 4 °C with anti-Pmp70 Guinea Pig polyclonal antibody (a gift from Kyu-Sun Lee, 1:500) diluted in PBST, followed by the incubation with secondary antibodies for 1 h at RT. After washes, tissues were mounted using ProLong Gold antifade reagent (Thermo Fisher Scientific) and imaged with an FV3000 Confocal Laser Scanning Microscope (Olympus). Hoechst 33342 was used for nuclear staining. For the quantification, the images were first processed and deconvoluted using Olympus CellSens Dimension software (Olympus). The number of punctae or fluorescent intensity/area in a selected region of interest (ROI) was measured using the CellSens. To quantify the punctae near the nucleus, we first selected ROIs surround the nucleus according to Hoechst signal, and then counted the punctae number within each ROI using the CellSens Measure and Count module. Two to four ROIs were analyzed for each image. The imaging quantifications were done single or double blind.

For peroxisomal import assay in human cells, Tet-PEX5^{C11A} cells were seeded in 24-well plates on coverslips (Neuvitro #GG1215PLL). After 1 day, cells were transfected with GFP-SKL plasmid using Effectene reagent (Qiagen) following the manufacturer's instructions. Next day, the cells were treated with or without Dox (1 µg/mL) for 2 days. The cells were fixed in 4% paraformaldehyde for 10 min, and rinsed with 1× PBS, then permeabilized in 0.5% Triton X-100 in PBS for 10 min. Cells were blocked in PBS containing 1% bovine serum albumin for 1 h at RT, then incubated with anti-PEX14 (Thermo Fisher Scientific, #10594-1-AP) diluted in PBS for overnight at 4 °C. Next day, cells were incubated with secondary antibodies (Alexa Flour 594 donkey anti-rabbit IgG [1:1,000] for 1 h at RT). After washes, cells were mounted using ProLong Gold antifade reagent (Thermo Fisher Scientific) and imaged with an FV3000 Confocal Laser Scanning Microscope (Olympus). Hoechst 33342 was used for nuclear staining. For the quantification, the number of punctae per cell was counted manually. The image quantifications were done double blind. See Key resources table for antibody information.

Western blotting

Tet-PEX5^{C11A} cells were seeded in 6-well plates. After one day, cells were treated with or without Dox for 3 days. The proteins were extracted in NP-40 cell lysis buffer (Thermo Fisher Scientific, #FNN0021) containing 1×protease inhibitor cocktail (Sigma). For fly samples, 10–15 adult female flies were homogenized and lysed in 20 mM Tris-HCl (pH 8.0), 100 mM NaCl, 5 mM β-mercaptoethonal, 1×protease inhibitor cocktail (Sigma). Protein samples were denatured with Laemmli sample buffer (Bio-Rad, #161-0737) at 95 °C for 5 min. Then proteins were separated by Mini-PROTEAN TGX Precast Gels (Bio-Rad). Following incubation with primary and secondary antibodies, the blots were visualized with Pierce ECL Western Blotting Substrate (Thermo Scientific). See Key resources table for antibody information.

Northern blotting

Tet-PEX5^{C11A} cells were grown on a 12-well plate (3.75×10^5 cells) with or without Dox (1 µg/mL) for 2–3 days. Total RNA was extracted using Trizol reagent. RNA was separated on a 1% agarose gel prepared with Tri/Tri buffer (30 mM triethanolamine and 30 mM tricine, pH 7.9) containing 1.2% formaldehyde and run in Tri/Tri buffer. RNAs were transferred to a positively charged nylon membrane (Sigma) and fixed by UV cross-linking. Membranes were prehybridized with ULTRAhyb Ultrasensitive hybridization buffer (Thermo) for 30 min at 65 °C. The DIG-labeled oligonucleotide probe was added and incubated for 1 h at 65 °C then overnight at 37 °C. After hybridization, the membranes were washed twice for 10 min in 2× SSC with 0.1% SDS and then washed twice for 5 min in 0.1×SSC with 0.1% SDS at 37°C. DIG-labeled probes were detected with CDP-Star, ready-to-use (Sigma), following the manufacturer's instructions.

To prepare northern blotting probes, synthetic DNA oligonucleotides were prepared by Integrated DNA Technologies (IDT) and resuspended to a final concentration of 100 µM in dH$_2$O. The probes used in this study were 5′ETS, 5′-CGGAGGCCCAACC TCTCCGACGACAGGTCGCCAGAGGACAGCGTGTCAGC −3′; ITS-1, 5′-GGCCTCGCCCTCCGGGCTCCGTTAATGAT-3′; 18S, 5′-CGGAA CTACGACGGTATCTG-3′. The oligonucleotide probes were 3′-end coupled to digoxigenin (DIG)-dUTP using DIG Oligonucleotide Tailing Kit, 2nd Generation (Sigma), following the manufacturer's instructions.

Puromycin incorporation assay

Protein synthesis was monitored by quantification of the incorporation of puromycin into nascent polypeptide chain as described previously (68). In brief, Tet-PEX5^{C11A} cells were incubated with or without 1 µg/mL of Dox for 3 days, following by addition of 10 µg/mL of puromycin (Sigma #P7255) for 10 min. Cells were lysed for western blotting using an antipuromycin antibody (Sigma, #MABE343, 1:25000) to label the newly synthesized proteins.

Cell fitness assay

2.5×10^4 Tet-PEX5^{C11A} cells were seeded in a 96-well plate. Next day, cells were transfected with 20 nM of siRNAs using Opti-MEM (Thermo, 31985062) and RNAiMAX (Thermo, 13778150) according to the manufacturer's instructions. After 3 h, cells were incubated with or without Dox (1 µg/mL) for 3 days, and the number of cells was counted manually. All siRNA molecules were obtained from (IDT, Coralville, IA, USA), see Key resources table.

Cell death assay

2.5×10^4 Tet-PEX5^{C11A} cells were seeded in a 96-well plate. The next day, cells were transfected with 20 nM of siRNAs using Opti-MEM (Thermo, 31985062) and RNAiMAX (Thermo, 13778150) according to the manufacturer's instructions. Cells were then incubated with or without Dox (1 µg/mL). After 3 days, cells were stained with a LIVE/DEAD Cell Imaging Kit (Thermo, R37601), according to the manufacturer's instructions, and imaged on an FV3000 Confocal Laser Scanning Microscope (Olympus).

Intracellular ROS measurement

Human Tet-PEX5^{C11A} cells were seeded on 35 mm culture dish. After recovered for 1 day, cells were treated with Dox (1 µg/µL) for 48 h. To scavenge ROS, 4 mM NAC was added 3 h before the Dox treatment. To measure the intracellular ROS level, cells were incubated with 10 µM of H$_2$DCFDA for 10 min in the dark at 37 °C, and then washed with Hanks' balanced salt solution. ROS levels were examined using a confocal microscope (FV3000, Olympus) with an excitation wavelength of 488 nm. Five different areas of cells were randomly selected from each sample, and the mean relative fluorescence intensity was measured for each group of cells.

Statistical analysis

Acknowledgments

Supplementary Material

Supplementary material is available at *PNAS Nexus* online.

Funding

Author Contributions

J.K., K.H., and H.B. conceptualized the project, designed the experiments, and wrote the paper. J.K. and K.H. performed most experiments and analyzed data. P.V. and T.M. performed part of the western blot analysis. J.C. and A.K. conducted the HEK293 cell fitness assay. M.S. provided the pairwise comparison analysis.

Preprints

This manuscript was posted on a preprint: Doi: https://doi.org/10.1101/2020.11.19.390609.

Data Availability

RNA-Seq data have been deposited to NCBI's GEO (Accession # GSE167197).

References

1 Alberts B, *et al.* 2002. The compartmentalization of cells. In: *Molecular biology of the cell.* 4th ed. Garland Science. p. 1694–1695.

2 Yoshida H. 2007. ER stress and diseases. *FEBS J.* 274(3):630–658.

3 Han J, *et al.* 2013. ER-stress-induced transcriptional regulation increases protein synthesis leading to cell death. *Nat Cell Biol.* 15(5):481–490.

4 Wrobel L, *et al.* 2015. Mistargeted mitochondrial proteins activate a proteostatic response in the cytosol. *Nature.* 524(7566):485–488.

5 Wang X, Chen XJ. 2015. A cytosolic network suppressing mitochondria-mediated proteostatic stress and cell death. *Nature.* 524(7566):481–484.

6 Weidberg H, Amon A. 2018. MitoCPR-A surveillance pathway that protects mitochondria in response to protein import stress. *Science.* 360(6385):eaan4146.

7 Boos F, *et al.* 2019. Mitochondrial protein-induced stress triggers a global adaptive transcriptional programme. *Nat Cell Biol.* 21(4):442–451.

8 Wanders RJ, Waterham HR. 2006. Biochemistry of mammalian peroxisomes revisited. *Annu Rev Biochem.* 75:295–332.

9 Baes M, Van Veldhoven PP. 2012. Mouse models for peroxisome biogenesis defects and β-oxidation enzyme deficiencies. *Biochim Biophys Acta.* 1822(9):1489–1500.

10 Fransen M, Nordgren M, Wang B, Apanasets O. 2012. Role of peroxisomes in ROS/RNS-metabolism: implications for human disease. *Biochim Biophys Acta.* 1822(9):1363–1373.

11 Waterham HR, Wanders RJ. 2012. Metabolic functions and biogenesis of peroxisomes in health and disease. *Biochim Biophys Acta.* 1822(9):1325.

12 Braverman NE, D'Agostino MD, MacLean GE. 2013. Peroxisome biogenesis disorders: biological, clinical and pathophysiological perspectives. *Dev Disabil Res Rev.* 17(3):187–196.

13 Waterham HR, Ebberink MS. 2012. Genetics and molecular basis of human peroxisome biogenesis disorders. *Biochim Biophys Acta.* 1822(9):1430–1441.

14 Kleiboeker B, Lodhi IJ. 2022. Peroxisomal regulation of energy homeostasis: effect on obesity and related metabolic disorders. *Mol Metab.* 65:101577.

15 He A, Dean JM, Lodhi IJ. 2021. Peroxisomes as cellular adaptors to metabolic and environmental stress. *Trends Cell Biol.* 31(8):656–670.

16 Huang K, *et al.* 2019. RiboTag translatomic profiling of *Drosophila* oenocytes under aging and induced oxidative stress. *BMC Genomics.* 20(1):50.

17 Narayan V, *et al.* 2016. Deep proteome analysis identifies age-related processes in *C. elegans. Cell Syst.* 3(2):144–159.

18 Kim JA. 2020. Peroxisome metabolism in cancer. *Cells.* 9(7):1692.

19 Ferreira AR, Marques M, Ramos B, Kagan JC, Ribeiro D. 2022. Emerging roles of peroxisomes in viral infections. *Trends Cell Biol.* 32(2):124–139.

20 Di Cara F, *et al.* 2019. Peroxisomes in immune response and inflammation. *Int J Mol Sci.* 20(16):3877.

21 Fabelo N, *et al.* 2011. Severe alterations in lipid composition of frontal cortex lipid rafts from Parkinson's disease and incidental Parkinson's disease. *Mol Med.* 17(9–10):1107–1118.

22 Du Y, *et al.* 2018. A genome-wide expression association analysis identifies genes and pathways associated with amyotrophic lateral sclerosis. *Cell Mol Neurobiol.* 38(3):635–639.

23 Baker A, Lanyon-Hogg T, Warriner SL. 2016. Peroxisome protein import: a complex journey. *Biochem Soc Trans.* 44(3):783–789.

24 Gould SJ, Collins CS. 2002. Opinion: peroxisomal-protein import: is it really that complex? *Nat Rev Mol Cell Biol.* 3(5):382–389.

25 Gould SJ, Keller GA, Hosken N, Wilkinson J, Subramani S. 1989. A conserved tripeptide sorts proteins to peroxisomes. *J Cell Biol.* 108(5):1657–1664.

26 Platta HW, Erdmann R. 2007. The peroxisomal protein import machinery. *FEBS Lett.* 581(15):2811–2819.

27 Francisco T, *et al.* 2017. Protein transport into peroxisomes: knowns and unknowns. *Bioessays.* 39(10):1–10.

28 Kim J, Bai H. 2022. Peroxisomal stress response and inter-organelle communication in cellular homeostasis and aging. *Antioxidants (Basel).* 11(2):192.

29 Giordano CR, Terlecky SR. 2012. Peroxisomes, cell senescence, and rates of aging. *Biochim Biophys Acta.* 1822(9):1358–1362.

30 Huang K, *et al.* 2020. Impaired peroxisomal import in *Drosophila* oenocytes causes cardiac dysfunction by inducing upd3 as a peroxikine. *Nat Commun.* 11(1):2943.

31 Legakis JE, *et al.* 2002. Peroxisome senescence in human fibroblasts. *Mol Biol Cell.* 13(12):4243–4255.

32 Sebastiani P, *et al.* 2021. Protein signatures of centenarians and their offspring suggest centenarians age slower than other humans. *Aging Cell.* 20(2):e13290.

33 Koepke JI, *et al.* 2007. Restoration of peroxisomal catalase import in a model of human cellular aging. *Traffic.* 8(11):1590–1600.

34 Rackles E, *et al.* 2021. Reduced peroxisomal import triggers peroxisomal retrograde signaling. *Cell Rep.* 34(3):108653.

35 Kovacs WJ, *et al.* 2009. Peroxisome deficiency causes a complex phenotype because of hepatic SREBP/Insig dysregulation associated with endoplasmic reticulum stress. *J Biol Chem.* 284(11):7232–7245.

36 Kovacs WJ, *et al.* 2012. Peroxisome deficiency-induced ER stress and SREBP-2 pathway activation in the liver of newborn PEX2 knock-out mice. *Biochim Biophys Acta.* 1821(6):895–907.

37 Hasan S, Platta HW, Erdmann R. 2013. Import of proteins into the peroxisomal matrix. *Front Physiol.* 4:261.

38 Okumoto K, *et al.* 2011. Cysteine ubiquitination of PTS1 receptor Pex5p regulates Pex5p recycling. *Traffic.* 12(8):1067–1083.

39 Gutierrez E, Wiggins D, Fielding B, Gould AP. 2007. Specialized hepatocyte-like cells regulate *Drosophila* lipid metabolism. *Nature.* 445(7125):275–280.

40 Mast FD, *et al.* 2011. A *Drosophila* model for the Zellweger spectrum of peroxisome biogenesis disorders. *Dis Model Mech.* 4(5):659–672.

41 Cox JS, Shamu CE, Walter P. 1993. Transcriptional induction of genes encoding endoplasmic reticulum resident proteins requires a transmembrane protein kinase. *Cell.* 73(6):1197–1206.

42 Dey S, *et al.* 2010. Both transcriptional regulation and translational control of ATF4 are central to the integrated stress response. *J Biol Chem.* 285(43):33165–33174.

43 Harding HP, Zhang Y, Bertolotti A, Zeng H, Ron D. 2000. Perk is essential for translational regulation and cell survival during the unfolded protein response. *Mol Cell.* 5(5):897–904.

44 Wek RC, Jiang HY, Anthony TG. 2006. Coping with stress: eIF2 kinases and translational control. *Biochem Soc Trans.* 34(Pt 1):7–11.

45 Harding HP, *et al.* 2000. Regulated translation initiation controls stress-induced gene expression in mammalian cells. *Mol Cell.* 6(5):1099–1108.

46 Haze K, Yoshida H, Yanagi H, Yura T, Mori K. 1999. Mammalian transcription factor ATF6 is synthesized as a transmembrane protein and activated by proteolysis in response to endoplasmic reticulum stress. *Mol Biol Cell.* 10(11):3787–3799.

47 Ryoo HD, Domingos PM, Kang MJ, Steller H. 2007. Unfolded protein response in a *Drosophila* model for retinal degeneration. *EMBO J.* 26(1):242–252.

48 Pakos-Zebrucka K, *et al.* 2016. The integrated stress response. *EMBO Rep.* 17(10):1374–1395.

49 Costa-Mattioli M, Walter P. 2020. The integrated stress response: from mechanism to disease. *Science.* 368(6489):eaat5314.

50 Sidrauski C, McGeachy AM, Ingolia NT, Walter P. 2015. The small molecule ISRIB reverses the effects of eIF2alpha phosphorylation on translation and stress granule assembly. *Elife.* 4:e05033.

51 Münch C, Harper JW. 2016. Mitochondrial unfolded protein response controls matrix pre-RNA processing and translation. *Nature.* 534(7609):710–713.

52 Quirós PM, *et al.* 2017. Multi-omics analysis identifies ATF4 as a key regulator of the mitochondrial stress response in mammals. *J Cell Biol.* 216(7):2027–2045.

53 Ben-Sahra I, Hoxhaj G, Ricoult SJH, Asara JM, Manning BD. 2016. mTORC1 induces purine synthesis through control of the mitochondrial tetrahydrofolate cycle. *Science.* 351(6274):728–733.

54 Park Y, Reyna-Neyra A, Philippe L, Thoreen CC. 2017. mTORC1 balances cellular amino acid supply with demand for protein synthesis through post-transcriptional control of ATF4. *Cell Rep.* 19(6):1083–1090.

55 Torrence ME, *et al.* 2021. The mTORC1-mediated activation of ATF4 promotes protein and glutathione synthesis downstream of growth signals. *Elife.* 10:e63326.

56 Sidrauski C, *et al.* 2015. Pharmacological dimerization and activation of the exchange factor eIF2B antagonizes the integrated stress response. *Elife.* 4:e07314.

57 Tsai JC, *et al.* 2018. Structure of the nucleotide exchange factor eIF2B reveals mechanism of memory-enhancing molecule. *Science.* 359(6383):eaaq0939.

58 Lange PS, *et al.* 2008. ATF4 is an oxidative stress-inducible, pro-death transcription factor in neurons in vitro and in vivo. *J Exp Med.* 205(5):1227–1242.

59 Roybal CN, Hunsaker LA, Barbash O, Vander Jagt DL, Abcouwer SF. 2005. The oxidative stressor arsenite activates vascular endothelial growth factor mRNA transcription by an ATF4-dependent mechanism. *J Biol Chem.* 280(21):20331–20339.

60 Harding HP, *et al.* 2003. An integrated stress response regulates amino acid metabolism and resistance to oxidative stress. *Mol Cell.* 11(3):619–633.

61 Itoh K, *et al.* 1997. An Nrf2/small Maf heterodimer mediates the induction of phase II detoxifying enzyme genes through antioxidant response elements. *Biochem Biophys Res Commun.* 236(2):313–322.

62 Wortel IMN, van der Meer LT, Kilberg MS, van Leeuwen FN. 2017. Surviving stress: modulation of ATF4-mediated stress responses in normal and malignant cells. *Trends Endocrinol Metab.* 28(11):794–806.

63 Hiramatsu N, *et al.* 2014. Translational and posttranslational regulation of XIAP by eIF2α and ATF4 promotes ER stress-induced cell death during the unfolded protein response. *Mol Biol Cell.* 25(9):1411–1420.

64 Elhamamsy AR, Metge BJ, Alsheikh HA, Shevde LA, Samant RS. 2022. Ribosome biogenesis: a central player in cancer metastasis and therapeutic resistance. *Cancer Res.* 82(13):2344–2353.

65 Baßler J, Hurt E. 2019. Eukaryotic ribosome assembly. *Annu Rev Biochem.* 88:281–306.

66 Ma XM, Blenis J. 2009. Molecular mechanisms of mTOR-mediated translational control. *Nat Rev Mol Cell Biol.* 10(5):307–318.

67 Iadevaia V, Liu R, Proud CG. 2014. mTORC1 signaling controls multiple steps in ribosome biogenesis. *Semin Cell Dev Biol.* 36:113–120.

68 Schmidt EK, Clavarino G, Ceppi M, Pierre P. 2009. SUnSET, a non-radioactive method to monitor protein synthesis. *Nat Methods.* 6(4):275–277.

69 Nathans D. 1964. Puromycin inhibition of protein synthesis: incorporation of puromycin into peptide chains. *Proc Natl Acad Sci U S A.* 51(4):585–592.

70 Hansen WJ, Lingappa VR, Welch WJ. 1994. Complex environment of nascent polypeptide chains. *J Biol Chem.* 269(43):26610–26613.

71 Zalckvar E, Schuldiner M. 2022. Beyond rare disorders: a new era for peroxisomal pathophysiology. *Mol Cell.* 82(12):2228–2235.

72 Teske BF, *et al.* 2011. The eIF2 kinase PERK and the integrated stress response facilitate activation of ATF6 during endoplasmic reticulum stress. *Mol Biol Cell.* 22(22):4390–4405.

73 Fusakio ME, *et al.* 2016. Transcription factor ATF4 directs basal and stress-induced gene expression in the unfolded protein response and cholesterol metabolism in the liver. *Mol Biol Cell.* 27(9):1536–1551.

74 Ohoka N, Yoshii S, Hattori T, Onozaki K, Hayashi H. 2005. TRB3, a novel ER stress-inducible gene, is induced via ATF4-CHOP pathway and is involved in cell death. *EMBO J.* 24(6):1243–1255.

75 Freed EF, Bleichert F, Dutca LM, Baserga SJ. 2010. When ribosomes go bad: diseases of ribosome biogenesis. *Mol Biosyst*. 6(3):481–493.

76 Turi Z, Lacey M, Mistrik M, Moudry P. 2019. Impaired ribosome biogenesis: mechanisms and relevance to cancer and aging. *Aging (Albany NY)*. 11(8):2512–2540.

77 Parlato R, Liss B. 2014. How Parkinson's disease meets nucleolar stress. *Biochim Biophys Acta*. 1842(6):791–797.

78 Hetman M, Pietrzak M. 2012. Emerging roles of the neuronal nucleolus. *Trends Neurosci*. 35(5):305–314.

79 Tafforeau L, *et al*. 2013. The complexity of human ribosome biogenesis revealed by systematic nucleolar screening of Pre-rRNA processing factors. *Mol Cell*. 51(4):539–551.

80 Szaflarski W, *et al*. 2022. Early rRNA processing is a stress-dependent regulatory event whose inhibition maintains nucleolar integrity. *Nucleic Acids Res*. 50(2):1033–1051.

81 Rozelle DK, Filone CM, Kedersha N, Connor JH. 2014. Activation of stress response pathways promotes formation of antiviral granules and restricts virus replication. *Mol Cell Biol*. 34(11):2003–2016.

82 Rabouw HH, *et al*. 2019. Small molecule ISRIB suppresses the integrated stress response within a defined window of activation. *Proc Natl Acad Sci U S A*. 116(6):2097–2102.

83 Fransen M, Lismont C, Walton P. 2017. The peroxisome-mitochondria connection: how and why? *Int J Mol Sci*. 18(6):1126.

84 Dirkx R, *et al*. 2005. Absence of peroxisomes in mouse hepatocytes causes mitochondrial and ER abnormalities. *Hepatology*. 41(4):868–878.

85 Baes M, Van Veldhoven PP. 2016. Hepatic dysfunction in peroxisomal disorders. *Biochim Biophys Acta*. 1863(5):956–970.

86 Peeters A, *et al*. 2015. Mitochondria in peroxisome-deficient hepatocytes exhibit impaired respiration, depleted DNA, and PGC-1α independent proliferation. *Biochim Biophys Acta*. 1853(2):285–298.

87 Hughes JL, *et al*. 1990. Pathology of hepatic peroxisomes and mitochondria in patients with peroxisomal disorders. *Virchows Arch A Pathol Anat Histopathol*. 416(3):255–264.

88 Mittal M, Siddiqui MR, Tran K, Reddy SP, Malik AB. 2014. Reactive oxygen species in inflammation and tissue injury. *Antioxid Redox Signal*. 20(7):1126–1167.

89 Shinde AB, *et al*. 2018. Mitochondrial disruption in peroxisome deficient cells is hepatocyte selective but is not mediated by common hepatic peroxisomal metabolites. *Mitochondrion*. 39:51–59.

90 Guo X, *et al*. 2020. Mitochondrial stress is relayed to the cytosol by an OMA1–DELE1–HRI pathway. *Nature*. 579(7799):427–432.

91 Natsume T, Kiyomitsu T, Saga Y, Kanemaki MT. 2016. Rapid protein depletion in human cells by auxin-inducible degron tagging with short homology donors. *Cell Rep*. 15(1):210–218.

92 Dobin A, *et al*. 2013. STAR: ultrafast universal RNA-seq aligner. *Bioinformatics*. 29(1):15–21.

93 Love MI, Huber W, Anders S. 2014. Moderated estimation of fold change and dispersion for RNA-seq data with DESeq2. *Genome Biol*. 15(12):550.

94 Subramanian A, *et al*. 2005. Gene set enrichment analysis: a knowledge-based approach for interpreting genome-wide expression profiles. *Proc Natl Acad Sci U S A*. 102(43):15545–15550.

95 Schmittgen TD, Livak KJ. 2008. Analyzing real-time PCR data by the comparative C(T) method. *Nat Protoc*. 3(6):1101–1108.